SEMINÁRIOS PPG-EM / UERJ 2017

PPG-EM UERJ 2017 SEMINARS

Programa de Pós-graduação em Engenharia Mecânica UERJ

SEMINÁRIOS PPG-EM / UERJ 2017

PPG-EM UERJ 2017 SEMINARS

Programa de Pós-graduação em Engenharia Mecânica UERJ

WWW.PPG-EM.ENG.UERJ.BR

Editado por Rachel Lucena (rachel.lucena@gmail.com), Leon Lima (matosleon@gmail.com) e Gustavo Anjos (gustavo.anjos@uerj.br). Reprodução é permitida sem restrições. O *layout* foi criado a partir do modelo LaTeX "The Legrand Orange Book", versão 2.1 (14/11/2015), sob a licença Creative Commons:

Capa: Cataratas de Foz do Iguaçú, imagem aérea. Foto de Marcello Arrambide.
Imagem obtida da página `http://wanderingtrader.com/iguazu-falls/`.

Foto dos cabeçalhos dos capítulos: Foto subaquática.
Imagem obtida da página `https://professor-falken.com/pt/tag/burbujas/`

Edited by Rachel Lucena (rachel.lucena@gmail.com), Leon Lima (matosleon@gmail.com) and Gustavo Anjos (gustavo.anjos@uerj.br). There are no restrictions for reproducing this material. The layout was created from the LaTeX template "The Legrand Orange Book", version 2.1 (14/11/15), under the Creative Commons license:

Cover: Iguazu Falls, aerial view. Photograph from Marcello Arrambide.
Extracted from `http://wanderingtrader.com/iguazu-falls/`.

Picture on chapter headers: Underwater photograph.
Extracted from `https://professor-falken.com/pt/tag/burbujas/`

September 28, 2018

Conteúdo / Contents

1. Introdução / Introduction

"Change is one of mankind's most mysterious creations. The factors that operate to cause it came into play when man produced his first tool. With it he changed the world forever, and bound himself to the artifacts he would create in order, always, to make tomorrow better than today. But how does change operate? What triggers a new invention, a different philosophy, an altered society? The interactive network of man's activities links the strangest, most disparate elements, bringing together the most unlikely combinations in unexpected ways to create a new world."

Esse trecho foi extraído do capítulo "The Legacy of Science", escrito por James Burke, dentro da obra "The impact of science on society", que também contém contribuições de Jules Bergman e Isaac Asimov (Burke, Bergman, and Asimov, 1985).

Tal como pontuado por Burke, existe um elemento motriz das mudanças tecnológicas que é a interação entre as atividades humanas. Um ambiente que proporcione o compartilhamento de descobertas, de resultados, de ideias é necessário para o desenvolvimento científico e tecnológico eficiente.

Este anuário reúne todos os trabalhos apresentados no âmbito dos Seminários do PPG-EM em 2017, que contou com a participação de 17 alunos de mestrado e doutorado do Programa, além de cinco convidados externos. No total

"Change is one of mankind's most mysterious creations. The factors that operate to cause it came into play when man produced his first tool. With it he changed the world forever, and bound himself to the artifacts he would create in order, always, to make tomorrow better than today. But how does change operate? What triggers a new invention, a different philosophy, an altered society? The interactive network of man's activities links the strangest, most disparate elements, bringing together the most unlikely combinations in unexpected ways to create a new world."

This text was extracted from the chapter "The Legacy of Science", written by James Burke, which is part of the book "The impact of science on society", which also contains contributions from Jules Bergman and Isaac Asimov (Burke, Bergman, and Asimov, 1985).

As pointed out by Burke, the interaction of man's activities is one of the driving forces of the technological changes. An environment which facilitates the share of discoveries, results and ideas is a necessary condition for an efficient scientific and technological development.

This book is a compilation of the works presented in framework of the PPG-EM 2017 Seminars, which counted with the participation of 17 master's and doctorate students of the Program and five external guest researchers. From

foram 22 trabalhos apresentados, dos quais 14 geraram mini-artigos, que compõem este material.

A coordenação do PPG-EM agradece a todos que contribuíram para mais esse ano de produção científica e incentiva todo pesquisador a se manter fazendo ciência objetiva e de alta qualidade.

the 22 works presented, 14 generated short-papers, which are also part of this material.

The coordination of PPG-EM thanks every one that contributed to one more year of scientific production and encourage every researcher to keep making objective and high quality science.

[BBA85] James Burke, Jules Bergman, and Isaac Asimov. *The impact of science on society*. NASA Scientific and Technical Information Branch, 1985 (cited on page 7).

Prof. Manoel Antônio F. C. Filho
(Coordenador do PPG-EM)

Prof. José Brant de Campos
(Vice-coordenador do PPG-EM)

2. Resumos / Abstracts

Neste capítulo são apresentados os resumos dos vinte e dois trabalhos científicos que fizeram parte dos Seminários do PPG-EM em 2017. Os resumos estão organizados segundo a data de apresentação.

This chapter presents the abstracts of the twenty two scientific works that participated in the PPG-EM Seminars in 2017. Abstracts are organized according to the date of presentation.

2.1 1° SEMINÁRIO / 24-jan

RESUSPENSION OF THE LIGHT FINITE SIZED PARTICLES IN POINT-PARTICLE DNS USING VIRTUAL WALL

Hyun Ho Shin
hhs82528@gmail.com
Faculdade Politécnica - Universidade de Assunção

Sediment Transport is a process involved in many natural and man-made applications. In order to predict the behavior of the sediment particles in this kind of applications, it is essential to understand the interaction between the sediment particles and the fluid turbulence, which can be studied using numerical simulations. One of the numerical simulation useful for this purpose is the point-particle Direct Numerical Simulation (DNS). In point-particle DNS, all the length scales of the fluid turbulence are solved using fine grids, and each particle is tracked individually. The point-particle DNS is valid for particles much smaller than the smallest fluid turbulence length scale, which is not the case of sand sediment in turbulent water flow. In this work, we study the validity of point-particle DNS of sediment transport in turbulent channel flow. We analyse the relative importance of different forces acting on the particles and we discuss the necessity of the inclusion of an additional model for the point-particle DNS. In this work, we perform point-particle

DNS of particle laden turbulent channel flow with Reynolds number 180 and 500, based on shear velocity and channel height, tracking 10^5 particles using one-way coupling. The particle size is comparable to the smallest turbulent scales, and the particle to fluid density ratio is slightly larger than 1.

2.2 2° SEMINÁRIO / 23-fev

ESTIMATIVA DE PARÂMETROS E VARIÁVEIS DE ESTADO DE MODELOS APLICADOS A NEURÔNIOS CITOMEGÁLICOS UTILIZANDO DADOS EXPERIMENTAIS DO PROTOCOLO DE TENSÃO FIXA

Diego Estumano
diegoestumano@hotmail.com
Universidade Federal do Pará

A epilepsia é uma síndrome bastante comum no mundo. Uma das razões para o desenvolvimento desta síndrome é a má formação do sistema neurológico, sendo que existem fortes indícios na literatura de que os neurônios que inicializam as crises convulsivas são os do tipo citomegálico. Sendo assim, esta tese foi desenvolvida com o objetivo de caracterizar as propriedades eletrofisiológicas de neurônios citomegálicos. Utilizou-se aqui dados reais da corrente transmembrânica de células humanas, obtidos com a utilização do protocolo de tensão fixa. Na simulação computacional considerou-se diferentes modelos matemáticos para a representação das dinâmicas dos íons de sódio, potássio e cálcio através da membrana extracelular e entre o citoplasma e o retículo endoplasmático. Através de técnicas estatísticas dentro de uma abordagem Bayesiana, como o Método de Monte Carlo via Cadeia de Markov (MCMC), Filtro de Partículas e Computação Bayesiana Aproximada (ABC), foram estimados os parâmetros e variáveis de estado de cada modelo proposto, bem como foi selecionado o melhor modelo para prever as correntes transmembrânicas obtidas experimentalmente. Com os dados experimentais, os modelos matemáticos propostos e as ferramentas matemáticas utilizadas, mostra-se que o mecanismo de autoindução de cálcio é extremamente importante na eletrofisiologia dos neurônios citomegálicos.

2.3 3° SEMINÁRIO / 12-mai

OpenFOAM®: UMA FERRAMENTA LIVRE DE SIMULAÇÃO CFD

Prof. Livia Jatobá
jatoba.iprj@gmail.com
Instituto Politécnico do Rio de Janeiro / IPRJ

A Dinâmica dos Fluidos Computacional (ou Computational Fluid Dynamics, CFD) consiste na solução numérica das equações que governam o escoamento de fluidos. Esta área do conhecimento ganhou importância, pois é uma técnica de predição adotada em diferentes projetos de engenharia: turbomáquinas, aeroespacial, automobilística e na indústria de processos, por exemplo. Os avanços dos recursos computacionais e o acesso a diferentes aplicativos para simulação CFD ampliaram o uso dessa técnica. Entretanto, a área concentra desafios importantes para difundir ainda mais o uso das simulações CFD, tais como, o desenvolvimento de modelos que representem a física com acurácia, técnicas numéricas que resolvam as equações com baixo erro e baixo custo computacional e, ampliar o acesso ao conhecimento na área. O OpenFOAM® é um software livre (código aberto e sem custo de licença) de simulação CFD compatível com processamento em paralelo, malha não-estruturada e com desenvolvimento maduro o suficiente compreendendo a solução para diferentes

tipos de escoamento. Por estes motivos, esta ferramenta tem papel importante nesta fase de expansão do uso das simulações CFD, tanto no âmbito da capacitação quanto no desenvolvimento de projetos de engenharia e pesquisa.

2.4 4° SEMINÁRIO / 22-mai

PROBABILISTIC MODEL-BASED PROGNOSTICS USING MESH-FREE MODELING

Prof. Stephen Ekwaro-Osire
stephen.ekwaro-osire@ttu.edu
Department of Mechanical Engineering / Texas Tech University

Improved system reliability and reduced maintenance cost are guaranteed if the prediction of remaining useful life (RUL) is deemed to be accurate. Energy systems, like wind turbines, are the primary beneficiaries of this achievement as they tend to suffer from an unexpected early life failure of components that resulted in loss of revenue and high maintenance costs. The issue of uncertainty in prediction of future state is yet a prevailing issue in prognostics and due attention is paramount. Hence, there is a need for establishing a comprehensive framework to quantify uncertainty in prognostics and this talk addresses this issue by considering a research question 'can uncertainty considerations improve the prediction of RUL?' The following specific aims were developed to answer the research question: (1) develop a meshfree cantilever beam with uncertainty in loading conditions, and (2) predict RUL reliably. A probabilistic framework was developed that efficiently predicts remaining useful life of a component using a combination of meshfree model and degradation model. To account for prediction uncertainty, modeling and loading uncertainties are quantified and incorporated in the framework. Some results will be presented.

2.5 5° SEMINÁRIO / 28-jun

MICROHARDNESS MEASUREMENTS OF HYDROXYAPATITE SYNTHESIZED USING CHICKEN EGGS SHELL PRECURSORS

Marcelo Vitor Ferreira Machado
marcelovfmachado@gmail.com
PPG-EM/UERJ

The proposal of this work is determine one of most important mechanical properties of brittle materials, the hardness. Our work brittle material is a Hydroxyapatite (HAP) synthesized using chicken eggs shells as precursors. Using a field emission scanning electron microscope, we have obtained the mean size of HAP particles and with a sample of this material, we have obtained HAP sample surface images using a stereomicroscope and finally, we could determine some preliminary Vickers microhardness measurements of this HAP sample, which were used to define an important experimental parameter, that is the indenter application force upon the sample surface. After that definition, we have measured the Vickers microhardness to HAP synthesized from chicken eggs shell and compared them with Vickers microhardness commercial HAP.

2.6 6° SEMINÁRIO / 05-jul

SIMULATION OF ENERGY PERFORMANCE OF BUILDINGS: COMPARISON OF COMPUTATIONAL TOOLS DOMUS AND ENERGY PLUS

Paulo Roberto Lopes do Nascimento
p_roberto@uol.com.br
PPG-EM/UERJ

Brazilian buildings account for approximately 40% of Brazil's annual electricity consumption. In Europe, North America and Asia, the buildings are subject to intense campaigns and measures aimed at reducing their energy consumption. In Brazil, in 2009, the Technical Requirements for the Quality of the Energy Efficiency Level of Commercial, Services and Public Buildings (RTQ-C) were instituted, in order to provide the country with a regulation that evaluates the energy performance of a building , through two methods: Prescriptive and Simulation.The simulation can evaluate the thermal and energetic performance of new and existing buildings, analyzing the different alternatives of architectural design, construction components, lighting systems and HVAC. But for this to happen, it must be incorporated into the design routine of architectural and engineering offices with computational tools that are simple to use by architects and engineers. The objective of this work is to evaluate the RTQ-C Simulation Method, through the comparative analysis of two simulation tools, EnergyPlus and Domus, in the simulation of an existing public building.

2.7 7° SEMINÁRIO / 12-jul

EROSION BY IMPACT OF SOLID PARTICLES IN DUPLEX STAINLESS STEEL UNS S32205

Antônio Carlos Araújo
antonioaraujo61@ymail.com
PPG-EM/UERJ

Duplex stainless steels are being increasingly used in applications that require a greater corrosion resistance than traditional stainless steels.Its applications in both,outdoor or submerged structures,motivate the studies on its performance in various situations,as in the case of exposure to erosive wear.This work studies the effects of erosion by impact of solides particles on surfaces of samples of duplex stainless steel UNS S32205,from the point of view of both aspects,morphological and topographycal .Polished surfaces of the samples were subjected to erosive attacks by alumina particles in air flow ,with different exposure times.These were examined by scanning electron microscopy,looking at the forms of wear obtained and the surface's roughnesses were measured,aiming to follow the evolution of the erosive process.It was made a more datailed examination of craters,for comparison with the proposed machanisms in models described in the literature and with the results of simutations by the finite elements method.In this aspect the method proved to be as effective as the tradittional methods of ballistic studies using single particles,as well as to be more comprehensive and economic.The measures of surface roughness and the statistics from derived data signaled the possibility of use of this tool to the evaluate the beginning of the effective loss of mass,which characterizes the erosion.

LIFE CYCLE COST EVALUATION OF A HIGH EFFICIENCY COMBINED CYCLE POWER PLANT INSTALLED IN RIO DE JANEIRO CITY WITH A TIC – GAS TURBINE AIR INLET COOLING SYSTEM IMPLEMENTATION

Paulo Roberto Cruz
paulo.cruz.turbo@gmail.com
PPG-EM/UERJ

The aim of this technical paper is to compare the performance results of a high efficiency 110 MW Combined Cycle Power Plant (CC) instaled in Rio de Janeiro City, equiped with 2 aeroderivative gas turbines + 1 steam turbine, operating with and without a GT air inlet cooling system (TIC). At GT nominal speed the air volume flow remains aproximately constant, however, the mass flow will vary depending on the air inlet temperature and humidity. Increasing the ambient air temperature lowers the density of the inlet air, thus reducing the air mass flow through the GT, and therefore decreasing considerably the power output (which is proportional to the mass flow). For this specific engine, each increment of 1 oC in the GT incoming air temperature results in a loss of 1% in GT output shaft power, and increasing in 0,031% the heat rate. For a 10-year scenario, 2007-2016, a temperature database will be elaborated , with the weighted mediun daily temperature in Rio de Janeiro City all over the year. In economic evaluation will be considered the total extra electric power produced by CCPP system using TIC system technology, pricing this energy based on ANEEL fees, and also the total cost for TIC system implementation, the payback period, internal rate and the net present value.

PREPARATION OF N-FUNCTIONALIZED GRAPHITIC CARBON BY CATALYST-FREE PYROLYSIS OF THE BIOMASS WASTES CHITOSAN AND CHITIN

Thatiana Crispim
PPG-EM/UERJ

Formaldehyde (FA) is a volatile organic compound considered one of the largest pollutants in indoor environments. Of predominant anthropogenic origin, it is a major irritant to the eyes and pharynx. The major concern of FA exposure, however, is related to IARC classification on group 1 – carcinogenic to humans - which raised great public awareness. In this context, developing a new material for FA detection has a global interest due to the large industrial use in several segments. Therefore, here we propose the use of a new carbonaceous material from the biomass wastes Chitosan and Chitin for the detection and adsorption of formaldehyde. Favorable carbonyl–chemical adsorbent interactions with formaldehyde can be expected due to the presence of N atoms on the carbon when using N-functionalized graphitic carbon. Following green chemistry principles, avoiding any unfriendly metal catalyst and using a single carbon and nitrogen source of inexpensive biomass wastes, chitosan and chitin will be muffle furnace heated or pyrolyzed.

2.8 8° SEMINÁRIO / 19-jul

ANALYSIS OF THE MICROCLIMATE OF SÃO CRISTÓVÃO AND ITS INFLUENCE IN HEATING SYSTEMS, VENTILATING AND AIR CONDITIONING (HVAC)

Marcelo Fernandes Melo Monteiro
marcelofmm@gmail.com
PPG-EM/UERJ

Design heating, ventilation and air conditioning (HVAC) standards as ASHRAE and ANBT NBR 16401 supply only one climatic data for almost all cities listed, collected from meteorological stations located in the airports. In Rio de Janeiro, both airports are located next to the sea. It is well known that urban areas are characterized by different microclimates and the formation of heat islands, with an increase in air temperature compared to the areas of low occupancy or rural. As soon as the cost of automated meteorological stations have decreased, more suitable climatic data have become available. On the other hand, HVAC designer use commercial software for thermal load calculation where it is comfortable to pre-select climatic data ready available, usually that mentioned in the design standards. This paper aims at evaluating the effect of using meteorological data from the Santos Dumont Airport instead of the closest climatic data on the thermal load calculation of a building placed in São Cristóvão neighborhood. After choosing the design criteria and calculating the typical design day the differences in the thermal load results were analyzed.

STUDY REFERENCE TO REQUERIMENTS FOR CARBON STEEL IN PRESSURE VESSELS WITH H2S SERVICE IN OIL REFINING UNITS

Juliana Modesto de Andrade Machado da Rocha
PPG-EM/UERJ

H_2S in its humid form is one of the main corrosive agents of the petrochemical industry due to its acid characteristic and its hydrogenating potential. The major part of this contaminant comes from the fluid itself or it is created during the refining process of the fluid arising from the decomposition of sulphur compounds. Refineries and process plants use mainly carbon steel when fabricating pressure vessels due to the positive proportion between cost/result of this material. The article presented herein aims not only at analyzing the damages mechanisms caused by hydrogen as a result from corrosion, but also the factors which have influenced this degradation process and the applicable material requirements regarding the vessels which could avoid possible failures arising from those mechanisms. The requirements stated on the N-1706 are analyzed in order to verify the influence of such requirements on the increase of the resistance of the material to the damages caused by hydrogen.

2.9 9° SEMINÁRIO / 25-out

ANALYSIS OF HEAT INTERACTION BETWEEN FINS AND VARIABLE THERMAL CONDUCTIVITY

Jonatas Motta Quirino
quirinojm@hotmail.com
PPG-EM/UERJ

This work describes the thermal profile of rectangular fin, perpendicular to its primary surface and in steady state, which dissipates heat by conduction, convection and thermal radiation. Neumann and Dirichlet boundary conditions are established, characterizing that heat dissipation occurs only on the fin faces, in addition to predicting that the ambient temperature is homogeneous. Heat transfer analysis is performed by computational simulations using appropriate numerical methods. The Finite Differences Method is applied to the problem formulation. For the real situation approximation, the thermal conductivity of the material is considered as a function of temperature at each point, which makes the equation that governs the nonlinear problem. It is considered the use of double fins, where their surfaces interact thermally, generating mutual effects. Finally, the

comparison of the results obtained with typical results proves that the assumptions of variable thermal conductivity, heat dissipation by thermal radiation and mutual interaction are crucial to obtain results that are closer to reality.

2.10 10° SEMINÁRIO / 08-nov

INFLUENCE OF DISPERSION OF GRAPHENE OXIDE AND REDUCED GRAPHENE OXIDE ON POLYURETHANE IN GAS PERMEATION

Alessandro Eronides de Lima Silva
alessandroero@gmail.com
PPG-EM/UERJ

The coating industry has been working to improve the surface properties as wear, adhesion and wettability. In this sense, polymer nanocomposites have attracted great interest both in academic and industrial increase of properties obtained with small amounts of nanoparticles added to the polymer matrix. The graphene oxide, combined with polymers, has shown an impermeable nanocomposite barrier to gases and liquids and from this perspective it has attracted a particular interest for applications on oil and gas industry. In many cases, nanocoating acts as protective film that may prevent future corrosion problems and extend the devices lifetime. Many works in the literature indicate an improvement in the dispersion of graphene with the use of the ultrasonic tip compared to other methods. In this work, we report the influence of dispersion of graphene oxide (GO) and reduced graphene oxide (RGO) on polyurethane for gas permeation, to endorse its use for chemical protection applications. We have produced graphene/polyurethane nanocomposites in different conditions and subsequently dispersed at different time intervals using a ultrasonic tip. The samples obtained have been tested in a permeation analysis system. The coating films were studied by scanning electron microscopy (SEM), optical microscopy, atomic Force microscopy (AFM) and Raman Spectroscopy. The parameters used in the ultrasonic tip have allowed a homogeneous dispersion condition for the nanocomposites with different concentrations of graphene/polyurethane and those were chosen to select the best permeability condition.

CHARACTERIZATION OF JOINT WELDED BY TIG AUTOGENOUS STEEL PROCESS UNS S32707 SIMULATING A HEAT EXCHANGER FOR OIL HEATING

Waleska Gonçalves
wal.goncalves1@gmail.com
PPG-EM/UERJ

Analysis of brazed joints of UND S32707 type stainless steel with different amounts of nitrogen, with the highest value being 5.5% compared to the amount considered standard in the industry of 2.5% in the protection gas in the autogenous TIG welding process through the measurement of hardness profiles, MEV, EDS and EBSD, and study of the corrosion resistance of the different welded joints through corrosion test by mass loss, according to ASTM G48 standard simulating conditions close to working heat exchangers in oil refineries, where the crude oil is used.

2.11 11° SEMINÁRIO / 22-nov

PREPARATION OF GRAPHITIC CARBON BY CATALYST-FREE PYROLYSIS OF IIGNIN TO REDUCE VOLATILE ORGANIC COMPOUND OF THE WORK ENVIRONMENT

Sérgio Leandro Soares Itajahy Pinto da Costa
leandroatalaia@poli.ufrj.br
PPG-EM/UERJ

In the last decades the chemical industry has intensified its efforts to reduce, prevent and eliminate the environmental impacts it has caused. At the same time, there is a growing concern for human well-being. Monitoring the work environment is increasingly common, thus ensuring the safety and health of the worker. Emissions of volatile organic compounds have motivated several research activities to develop efficient and low cost technologies for their capture. The preparation of a carbonaceous material from lignin, the second most abundant biopolymer in the nature and sub product of the paper industry, appears as an alternative to this demand. Mesoporous graphitic materials can be obtained from lignin pyrolysis at 800 °C and deposited in polymer matrices or quartz plates for the physical adsorption of these harmful substances.

MATERIALS SELECTION USING GENETIC ALGORITHM

Thiago Carvalho Brito
PPG-EM/UERJ

In this work will be introduced a new tool, the Genetic Algorithm (GA), to improve quantitative methods for materials selection. The GA came from Biology and can be found in a toolbox of Matlab. Presently, it is increasingly used in engineering, mainly in structural optimization, but not in the area of material selection, where apparently it could be useful. Two quantitative methods, Ashby charts and CES Software, were used with Genetic Algorithm to select the fittest material for a case study, a blade of a TIDAL Turbine, and their results are compared.

MAGNETIC CYCLES OF THE SUN AND ITS IMPACTS ON THE NATURAL PHENOMENA OF THE EARTH

Lorena Albuquerque Santos
PPG-EM/UERJ

This work aims to find a possible correlation between the magnetic cycles of the Sun and some natural phenomena, such as intense and prolonged droughts, mainly those caused by phenomena such as El Niño and La Niña. The dry season will not be considered in this work. The sun is a great mass of activity. With each period that lasts about 11 years, there is what is called the solar cycle. Within these cycles, there are two very important periods: the maximum and minimum solar. In the first period solar activities reach their highest point, ending the cycle. During the solar minimum, the sun does not become monotonous. Quite the opposite. During the minimum, it is possible to perceive some places where the magnetic field of the Sun opens, allowing the flow of particles, that affect Earth, causing geomagnetic storms. And how can these storms, which during solar minimums prove to be so disturbing and reach their summit during their solar maximum, really can intensify the natural phenomena of the Earth? It is hoped that questions like these and so many others will be answered at the end of this paper.

2.12 12° SEMINÁRIO / 06-dez

STUDY OF EROSION BY IMPACT OF SOLID PARTICLES ON METALLIC COATING OBTAINED BY THERMAL ASPERSION

Márcio Cossenza
marciocossenza@uol.com.br
PPG-EM/UERJ

The objective of this work is to evaluate the feasibility of using a metallic coating inside acquatubular boilers. A thermal spray coating process is applied to the external surfaces of pipe walls, where the heat exchange takes place, between the boiler furnace and the water inside the pipes. An overview of the importance of power generation from coal-fired power plants is analyzed, as well as a brief study on the properties of boilers and mineral coal fuel. The electric arc thermal spray process, applied in the samples available for this work, uses a metal alloy developed in partnership with specialized companies to obtain a final product that is resistant to the corrosion and abrasive wear from coal ashes, with good adhesion to the steel substrate. The alloy also must present thermal conductivity compatible with the substrate conductivity, thermal expansion coefficient compatible with the substrate expansion coefficient, and easy application in the field to enable a feasible application procedure. In the evaluation of such performance, international standards are used to allow comparison with results already obtained in other works developed around the world. The test devices and equipment used are compatible with the procedures and standards used for the experiments.

MANUFACTURE OF NANOPOSITIONERS FOR SCIENTIFIC AND INDUSTRIAL APPLICATIONS

Rodrigo Sena Barbosa Leite
rodrigoleite@mecanica.coppe.ufrj.br
PPG-EM/UERJ

This project proposes the development and manufacture of a nanopositioning device for instrumentation in microscopy and spectroscopy in low temperature and ultra high vacuum conditions. The main idea of the project is integrate applied science in the development of a device with great future marketing potential and basic science, creating conditions for scientific discovery in nanoscience by the use of this device in probe and electronic microscopes. The innovative potential of the device will allow the development of a high value-added nanotechnology product in an industry still incipient in Brazil.

CHARACTERIZATION AND PERFORMANCE ANALYSIS OF AISI 1045 STEEL TOOL WITH TiN THIN FILM OF FSW WELDING PROCESS

Paulo Rodrigues Oliveira
rodrigues.oliveira@marinha.mil.br
PPG-EM/UERJ

The Friction Stir Welding (FSW) process, consists in the union of materials, dissimilar or not, with the use of a rotating tool. During this process doesn't have fusion of the involved materials. For this a series of defects, from the welding process, are eliminated. The tool responsible for the penetration, friction and formation of the weld bead requires a serious method of selection

to obtain a viable cost-benefit ratio. The objective of this work is to characterize the superficial coating performed in tools for the FSW process aiming at the increase in tool life, improvements in the welding parameters and reduction in the cost of the materials used for the fabrication. To perform this work will be used samples of AISI 1045 steel coated, through deposition of thin films by the Sputtering method, with TiN, in inert atmosphere. X-ray diffraction (XRD) techniques, X-Ray excited photoelectron spectroscopy (XPS) and nanoindentation techniques will be used to characterize the TiN Film. In additional welding processes will be realized to compare a tool with and without TiN film. In this way, we intend to improve the manufacturing of tools for the FSW process through processes currently existing in the machine tool industry.

NUMERICAL SOLUTION FOR TWO-DIMENSIONAL NONLINEAR PROBLEMS IN STEADY STATE

Caroline Alves
PPG-EM/UERJ

Currently two-dimensional nonlinear heat conduction problems do not have simple solutions through classical mathematical methods; with this, the approach procedures are more used. This work aims to present a proposal of a numerical solution for nonlinear problems, that is, where K depends on temperature, in a permanent regime without internal heat generation. The main idea is to use the Finite Differences Method to calculate these problems in a rectangular region, using software.

2.13 13° SEMINÁRIO / 13-dez

EXPERIMENTS AND CFD SIMULATIONS ON POOL BOILING AND TWO-PHASE FLOWS

Emanuele Teodori
Instituto Superior Técnico de Lisboa

Pool boiling and two-phase flows such as flow boiling in micro-channels and droplet impact onto a heated surface involve complex mechanisms of heat transfer due to the presence of a Vapour/Liquid/Solid interface. One can act in fact on the interface in order to alter the heat transfer removal of system based on two phase flows. In this context the work presented focused on effect of two surface topography alteration techniques on the pool boiling heat transfer. The first technique consisted in micro structuring surfaces with arrays of micro-cavities while the second consisted on extreme modification of the wettability of the surface. Surfaces with micro cavities were found useful for the final realization of an optimized two phase cooler for CPU, while extreme wettability scenarios resulted in a completely unexpected boiling behaviour. However experimental work in two phase flows requires complex instrumentation and massive experimental campaigns. To tackle these issues CFD reproduction of two phase flows can on one side reveals micro-scale physics involved in two phase flows, while on the other side can be a powerful tool to perform numerical experiments. In this context CFD simulations of droplet impact onto a surface, slug flow in microchannel and pool boiling are briefly presented and the obtained calculated results are compared versus performed experiments to benchmark the proposed numerical solvers for two phase flows.

3. Artigos compactos / Short papers

Quatorze dos vinte e dois trabalhos são apresentados em artigos compactos, que podem ser lidos neste capítulo.

Fourteen of the twenty two works are presented as short papers, which can be read in this chapter.

LISTA DE ARTIGOS COMPACTOS / LIST OF SHORT PAPERS:

	phenomena of the Earth
Márcio Cossenza	Study of erosion by impact of solid particles on metallic coating obtained by thermal aspersion
Rodrigo Sena Barbosa Leite	Manufacture of nanopositioners for scientific and industrial applications
Paulo Rodrigues Oliveira	Characterization and performance analysis of AISI 1045 steel tool with TiN think film of FSW welding process

Microhardness Measurements of Hydroxyapatite Synthesized Using Chicken Eggs Shell Precursors

Author: Marcelo Vitor Ferreira Machado[1] *marcelovfmachado@gmail.com*
Advisor: José Brant de Campos[1]

1State University of Rio de Janeiro

PPG-EM Seminars: season **2017**
www.ppg-em.uerj.br

July 05, 2017

Keywords: Hydroxyapatite, Microhardness, Chicken Eggs Shell.

1 Introduction

Considering the advance in the biocompatible materials researches, hydroxyapatite (HAP) have been revelead a important alternative to bone grafts and orthodontic implants. Because of its similarity with inorganic phase of bone tissues and its osteoconducting property [1], HAP is a brittle material that it doesn't show rejections.

In general, one of the most important features for those applications is the search to the improvement of the sintered HAP mechanical properties, obtained by the use of different chemical methods and precursor materials. Concerning microhardness measurements, other mechanical properties can be determined from them, for example, fracture toughness (KIC) and an analysis of the strain hardening effects[2], in the plastic behavior.

2 Materials and Methods

A Field Emission Scanning Electron Microscope (JEOL JSM 7100F) has been used to obtain the mean size of hydroxyapatite particles.

Samples of hydroxyapatite could be conformed by uniaxial compression method using a uniaxial hydraulic press equipment (Contenco Pavitest), where we have used a average compression force equal to 4000 kgf for 20 minutes, that provide an average stress compression of approximately 77.44 MPa during that time. The sintering process have been made in a QUIMIS (Mufla Stove) during 2 hours at 1000 °C. Theses equipments have been used to determine the experimental parameters that would be for comparison between chicken eggs shell HAP and comercial HAP.

HAP samples has been tested in a microhardness equipment (Pantec HDX-1000TM) to define the indenter force experimental parameter (200 gf) during 15 s and determine some preliminary Vickers microhardness measurements of this HAP sample. Finally, we have acquired a stereomicroscope (Discovery.V8 ZEISS) image of the HAP specimen's surface, on which we could note some irregularities and impurities. Theses equipments have been used to determine the experimental parameters that would be for comparison between chicken eggs shell HAP and comercial HAP.

To determine the microhardness of HAP samples for that comparison, the only change have been in hydraulic press equipment. Samples of hydroxyapatite could be conformed by uniaxial compression method using a uniaxial hydraulic press equipment (EVA 5052), where we have used a average compression force equal to 4000 kgf for 20 minutes, that provide an average stress compression of approximately 254.91 MPa (this samples have been compressed using a more narrow matrix than one) during that time.

3 Results

The experimental parameters to Vickers microhardness test determined have been 200 gf to indenter force (among 50 gf, 100 gf and 200 gf, this last parameter has shown the best microhardness impression) and 15 s to the time indentation.

After those experimental determination, the microhardness measurements in chicken eggs shell HAP and commercial HAP have been measured. To the chicken eggs shell HAP the measures have been determined using 6 samples and the results are:

Average: 35.846 HV

Standard Deviation: 4.198

Amplitude: 19.347 HV

Then, to the commercial HAP microhardness measures, 3 samples have been used and the statistics data are:

Average: 40.860 HV

Standard Deviation: 5.952

Amplitude: 21.503 HV

3.1 Graphics

Histograms relating the number of measures (vertical axis) with the respectives Vickers microhardness range to each kind of HAP (horizontal axis) have been plotted as shown below:

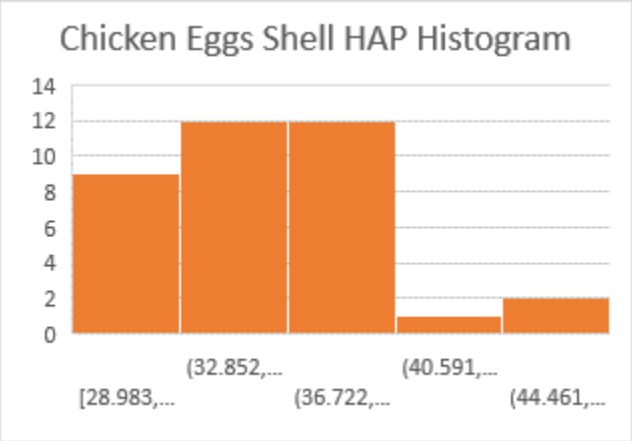

Figure 1: Chicken eggs shell HAP histogram.

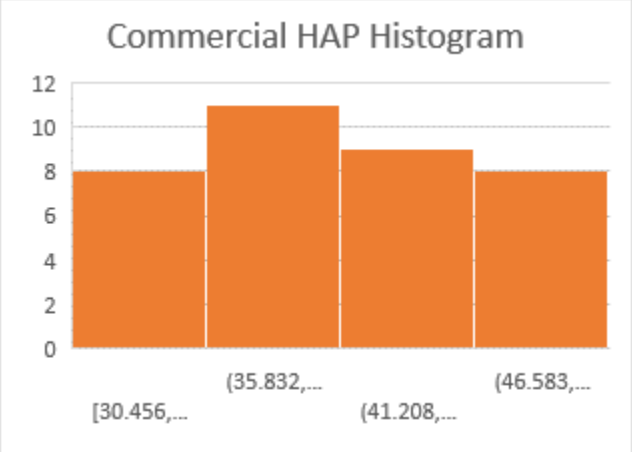

Figure 2: Commercial HAP histogram.

4 Conclusions

The research is going on using the indenter force experimental parameter defined (200 gf) upon the hydroxyapatite samples to determine microhardness measurements as we can observe in the sequence.

Then, doing a simple statistics data analysis we can observe that the commercial HAP microhardness average is greater than chicken eggs shell HAP microhardness average, as we have already expected, but the measurements to comercial HAP microhardness show a greater dispersion around the average than chicken eggs shell HAP. The value of standard deviation obtained to the commercial HAP samples is great enough to contemplate the chicken eggs shell HAP samples average.

This research is ongoing with other experiments to analyse why this microhardness behavior to chicken eggs shell have been shown.

5 Acknowledgments

The author would like to give a special thanks for the advisor of this research José Brant de Campos and all members of our hydroxyapatite research group, they are: Vitor S. Ramos, Marilza S. Aguilar, Bruno Di Lello, Saulo Acioli and Nataly Cristiane de Campos.

References

[1] Andrade, A. L., "Synthesis, *Caracterization, Tests and Use of HAP-91 Obteined from Calcite*" (1998).

[2] G. Muralithran, S. Ramesh, Ceramics International 26 (2000) 221 – 230.

[3] Th. Zisis, A. E. Giannakopoulos, International Journal of Solids and Structures 48 (2011) 3217 – 3231.

[4] D. B. Marshall, B. R. Lawn, Journal of Materials Science 14 (1979) 2001 – 2012.

[5] S. S. Scherrer, J. Robert Kelly. G. D. Quinn, K. Xu, Dental Materials 15 (1999) 342-348.

[6] Gomes L. C., Di Lello, B. C., Campos,J. B., Sampaio, M. A., *" Synthesis and Calcium Phosphate Caracterization Using Chicken Eggs Shell as Precursor"*

[7] Ferreira, J. R. M., da Rocha, D. N., Louro. L. H. L., Prado da Silva, M. H., *"Phosphating of Calcium Carbonate for Obtaining Hydroxyapatite from the Ostrich Egg Shell"*

Simulation of energy performance of buildings: comparison of computational tools Domus and EnergyPlus

Author: Paulo Roberto Lopes do Nascimento[1] *p_roberto@uol.com.br*
Advisors: Manoel Antônio Fonseca da Costa Filho[1] and Joyce Correna Carlo[2]

1 State University of Rio de Janeiro
2 Federal University of Viçosa

PPG-EM Seminar season 2017
www.ppg-em.uerj.br

July 05, 2017

Keywords: Energy efficiency, Labeling, Building Simulation

1 Introduction

Worldwide, buildings are responsible for approximately 40% of energy consumption [1]. In Europe, North America and Asia, they are subject to intense campaigns and legal measures, with the objective of making them more efficient in their energy consumption.

In Brazil, the type of energy most used in buildings is electricity, which is mainly generated in hydroelectric plants [2] and its increasingly consumption provides a greater share of thermal generation.

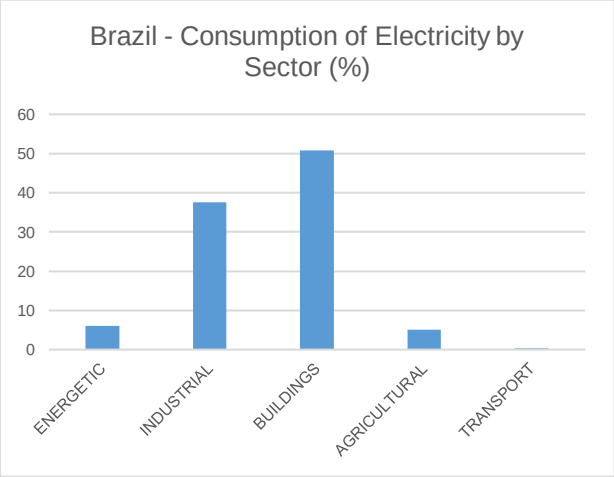

Fig. 1: Consumption of electricity I Brazil by sector.

The Technical Requirements for the Quality of the Energy Efficiency Level of Commercial, Services and Public Buildings (RTQ-C) [3][4] has the objective of providing evaluation mechanisms based on minimum performance criteria, using two methods to evaluate the energy performance of a building: the prescriptive and simulation.

1.2 Simulation

A building can be compared to a machine whose energy performance can be optimized [5]. However, the determination of the energy performance is not trivial task, since it involves a great amount of interdependent variables, whose mathematical modeling is complex.

Energy building simulation can evaluate the thermal and energetic performance of new and existing buildings, analyzing the different alternatives of architectural design, construction components, lighting systems and air conditioning [6].

Simulation is a process of experimenting with a detailed model of a real system to determine how it will respond to changes in its structure, environment or boundary conditions [7]. The large number of variables, the need for dynamical behavior analysis and repeated calculations to analyze the design alternatives leads to the use of computational tools to guide the evaluations under study. Currently, there are several simulation tools, among them Domus, developed by the Laboratory of Thermal Systems (LST) of PUC-PR, with agreement of Eletrobras and EnergyPlus, developed by U.S. Department of Energy (US DOE).

2 Methodology

The RTQ-C Simulation Method will be evaluated through the comparative analysis of two simulation tools, EnergyPlus and Domus, simulating an existing public building located at Santos Dumont Airport Area.

The methodology to develop the present work is that of the RTQ-C Simulation Method, which comprises:

- Modeling the actual building (baseline), with all the characteristics.
- Modeling the referenced building according to the required energy efficiency levels (A, B, C and D).

- The consumption of the proposed (actual) project is compared with the consumption of the reference project from the levels of A (most efficient) to E (less efficient). It must be demonstrated that the energy consumption of the proposed project must be equal to or less than the reference building of each level, which will determine the level of energy efficiency of the building.

- For buildings with simulation for natural ventilation will also be analyzed the percentage of hours occupied in comfort (POC).

3 Results

The expected results of this project are:

- Determination of energy efficiency level of the building with the two simulation tools.

Fig. 2: Inmetro's ENCE Label.

- Evaluation and comparison of the inputs and outputs datas required by the two simulation tools.

- Evaluate if the RTQ-C Simulation Method is easy to understand for use in architectural and engineering project offices.

4 Conclusions

In addition to assessing the energy efficiency level of a building, the RTQ-C Simulation Method can contribute to the cost-benefit decision-making of design solutions in relation to economic viability and energy consumption.

However, in order for it to be used intensively, it is necessary to carry out studies, developed with academic level treatment, for its dissemination to the Civil Construction stakeholders of buildings segment.

5 Acknowledgements

The author would like to give a special thanks for the advisor and co-advisor of this research, Manoel Antônio Fonseca Costa Filho and Joyce Correna Carlo and all members of Thermal and Energy Laboratory (UERJ) and Technology Laboratory in Environmental Comfort and Energy Efficiency (UFV).

6 References

[1] WORLD BUSINESS COUNCIL FOR SUSTAINABLE DEVELOPMENT. Energy efficiency in buildings – final report. WBCSD, 2007.
[2] EPE. Anuário estatístico de energia elétrica 2016. Empresa de Pesquisa Energética. Rio de Janeiro, 2016.

[3] INMETRO. Requisitos Técnicos da Qualidade do Nível de Eficiência Energética de Edifícios Comerciais, de Serviços e Públicos. Instituto Nacional de Metrologia, Normalização e Qualidade Industrial. Rio de Janeiro, 2010.

[4] INMETRO. Manual para Aplicação dos Regulamentos: RTQ-C e RAC-C. Instituto Nacional de Metrologia, Normalização e Qualidade Industrial. Rio de Janeiro, 2012.

[5] LOMARDO, Louise L. B. Estudo para uma regulação de estímulo à eficiência energética dos edifícios. Rio de Janeiro: UFRJ; COPPE, 2000.

[6] LAMBERTS, Roberto; DUTRA, Luciano e PEREIRA, Fernando O. R. Eficiência Energética na Arquitetura 3ª edição. Eletrobrás/Procel. Rio de Janeiro, 2014.

[7] HARREL, Charles R.; MOTT, Jack R.A.; BATEMAN, Robert E.; BOWDEN, Royce G.; GOGG, Thomas J. Simulação: Otimizando os sistemas. 2. ed. São Paulo: IMAM, 2002. 135 p.

EROSION BY IMPACT OF SOLID PARTICLES IN DUPLEX STAINLESS STEEL UNS S32205

Author: Antônio Carlos Araújo[1] *antonioaraujo61@ymail.com*
Advisor(s): Antonio Marinho Junior[1]
[1] Rio de Janeiro State University

July 1, 2015

PPG-EM Seminars: season **2017**
www.ppg-em.uerj.br

Keywords: Erosion, Duplex Stainless Steel, Morphology and Topography of surfaces.

1 Introduction

Due to economic losses related to the deterioration of engineering materials in-service, the study of Tribology has been receiving increasing attention from researchers in the field of mechanics and materials. In the case of wear by erosion, that caused by the impact of hard particles on surfaces of ductile metallic materials still offers opportunities for research, especially on the mechanisms that can explain the phenomena related to the loss of mass that characterizes erosion[1,2,3]. This work aims to study the morphological and topographical effects of erosion on a flat UNS S32205 duplex stainless steel, by means of individual and successive impacts of alumina particles. For these purposes, surfaces were examined by SEM and the roughness was measured by a digital profilometer.

2 MATERIALS AND METHODS

2.1 Target material

Figure 1: Blasting chamber and compressor.

In view of the objective of the work a planning was made to obtain results in the more economic and fast mode possible. It was designed and mounted an installation aimed to promote erosive wear in metallic surface, by the impact of hard particles. The most of the experiments described in literature [3, 4] uses spherical particles of hard material, impacting the surfaces examined. Here, a particles beam embedded in air flow, typical of industrial sand blasting procedures was used. The installation, specially designed and constructed for this project (Figure 1), consisted of a compact blasting chamber, coupled to a compatible air compressor.

Samples of stainless steel duplex UNS S32205 were removed from 1/2" thickness commercial plates manufactured by North American Stainless and provide by Expander. Mechanical properties of the material are: Yield stress (0,2 %): 586 MPa; Ultimate tensile stress: 784 MPa; Elongation in 50 mm: 34 % and Hardness: 20 HRC [4].

2.2 Impacting Particles

Alumina particles (Al2O3) produced by ALCOA and provided by ESSENCE with 100 Mesh average granulometry and variable morphology are shown in Figure 2:

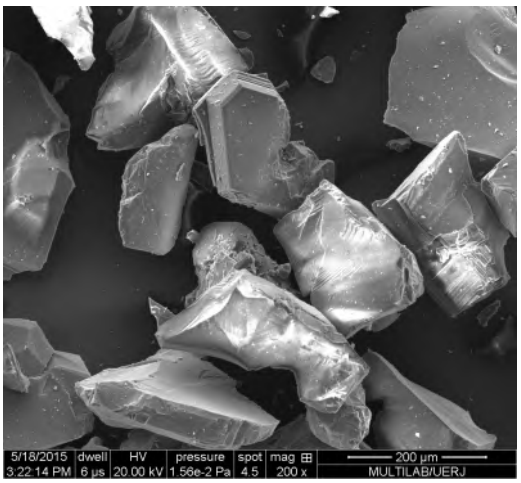

Figure 2: General aspect of Alumina particles.

3 RESULTS

The results with brief analyses are shown in tables of Figures 3 and 4. Each table includes a SEM micrography and a rugosimetric profile of the surface examined. Statistical curves from profiles are also included, as the ADC - Amplitude Distribution Curve and Abbott-Firestone (BAC - Bearing Area Curve).

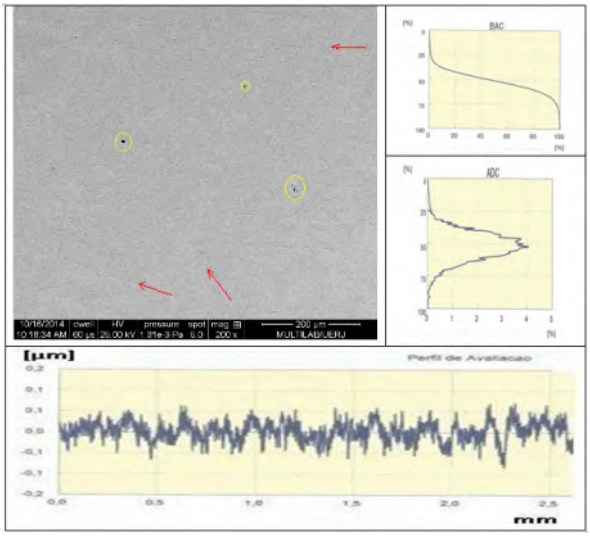

Figure 3: Polished sample. Micrography by SEM.

Morphological analysis: SEM image typical of polished surfaces. Scratches from grinding (red arrows). Voids revealed by polishing process (yellow circles). Topographical analysis: Roughness profile typical of polished surfaces. Gaussian distribution of ADC curve characterizes uniformity of surface finishing. Tips of the sigmoid BAC curve indicate equivalence between peaks and valleys in the profile [5].

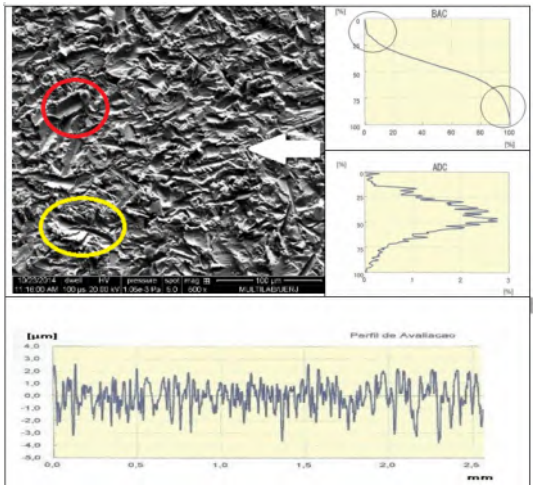

Figure 4: Sample after 3 s of erosive attack. Micrography by SEM.

Morphological analysis: SEM image showing craters. The crater pointed by white arrow (flux orientation) is elongated and oriented accordingly. The yellow and red circles show craters with borders due to plastic deformation [3, 4]. Different orientations were attributed to the turbulent nature of the flux. Topographical analysis: Roughness profile shows up to 3,7 micrometers of crater's depth and borders of 3 micrometers medium height. ADC curve was shifted to the left indicating more valleys than peaks. This is confirmed by the tips areas of BAC curve [5].

4 CONCLUSION

On the basis of the experiments carried out on samples of stainless steel UNS S32205 under the conditions established, it was possible to conclude:

The morphological study by SEM images of the surfaces of the material impacted by alumina particles conducted in turbulent air flow can be done in this way and not only with the use ballistic tests with a single particle.

This method allows obtaining simultaneously different shapes, sizes and orientations of surface craters, reducing the time and cost of the experiments.

The morphology of the craters formed on the surface of the material is compatible with models of erosion by cutting and plastic deformation, as well as experimental results of the literature consulted.

References

[1] JARJOURA,G,; Conference on Materials Degradation and Control,(in) Dalhouse University, Canada (2010).

[2] STACHOVIAK,G.H, Engineering Tribology, Elsevier, Amsterdam, 2Ed. Chap.1, pp1-9 (1993).

[3] SHEWMON AND SANDARARAJAN, The erosion of Metals, Ann. Rev Mat. Sci. (13) 301-18, (1983)

[4] AQUARO and FONTANI, Erosion of Ductile and Brittle Materials, Mecanica, 36 651-661, (2001)

[5] MATOS Jr, R.F. , Análise Topográfica da Superfície de Cilindro de Motores de Combustão Interna - Dissertação de Mestrado, UTFPr, Curitiba, 2009.

LCC Evaluation of a High Efficiency Combined Cycle Power Plant Installed In Rio de Janeiro City With a TIC – Gas Turbine Air Inlet Cooling System Implementation

Author: Paulo Roberto Cruz [1] *Paulo.cruz.turbo@gmail.com*

Advisor: Daniel José Nahid Mansur Chalhub[1]

1State University of Rio de Janeiro

PPG-EM Seminars: season 2017

Aug 29, 2017

www.ppg-em.uerj.br

Keywords: *Turbine Inlet Air Cooling System, Combined Cycle Power Plants, Aeroderivative Gas Turbines*

1. INTRODUCTION

A Life Cycle Cost evaluation will be performed of a high efficiency 110 MW Combined Cycle Power Plant operating in Rio de Janeiro City with the implementation of a TIC - Gas turbine air inlet cooling system. It will be determined the NPV for 20 years, considering: the extra power provided by GT and pricing under ANEEL fees [15], the ST power losses, and all costs involved for TIC system implementation.

The GT – Gas turbine performance is expressed in terms of net power available on the GT output shaft and heat rate. [2] [3] In GT at nominal speed the air volume flow remains approximately constant, however, the mass flow will vary depending on the air inlet temperature and humidity. Each increment of 1 ^{o}C in the GT incoming air temperature results in a loss of 1% in GT output shaft power, and increasing in 0,031% the heat rate. AC – Absorption chiller – TIC technology was elected as being the best technology to be applied.

1.2 A schematic diagram of the CCPP system + TIC

Figure 1. CCPP system schematic diagram to be installed in Rio de Janeiro City. The GT packages performance will be improved using 2 x 50% configuration AC - Absorption Chillers. These chillers will produce chilled water. Each AC uses heat input from a low-pressure steam (about 4.2 bar) from HRSG. The chilled water storage tank – TES will be installed between the AC and the chiller coil module. The primary pumps circulate chilled water between the chilled water storage tank and the absorption chiller, and the secondary pumps circulate chilled water between the TES - storage tank and the chiller coil module installed in front of GT air inlet filters.

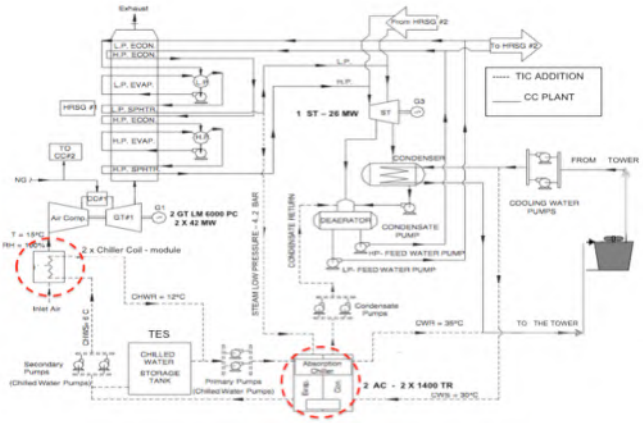

Figure 1 - CCPP + TIC schematic diagram

2. METHODOLOGY

2.1 On site ambient temperature election

For a 10 years scenario, 2007-2016, a temperature database was developed based on the collection of the hourly temperature measurements of the automatic meteorological station of Seropédica – RJ.

In one day the air temperature and humidity can vary greatly. Comparing a large number of the thermal amplitude samples during the days, it was observed a relative number of hours for the maximum, minimum and average temperatures, as given: 00:00 am to 8:00 am – minimum records, from 12:00 am to 6:00 pm – maximum records, and 9:00 am to 12:00 am / 7:00 pm to 11:00 pm – average records. [14] Therefore, for a same day, during the GT power calculation it will be considered the machine operating a amount of hours in maximum, avarage and minimum temperatures.

Figure 2. Meteorological station of Seropédica - RJ, located in the industrial area of Rio de Janeiro City.

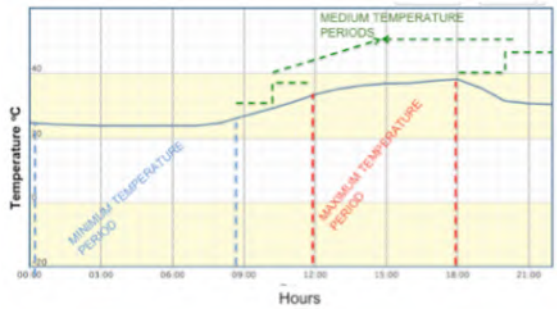

Figure 2. A day thermal amplitude [14]

2.2. Load calculation - cooling system dimensioning

The inlet air-cooling system, with absorption chiller (AC), will be dimensioned to cool the GT inlet air mass flow temperature from 32 °C to 15 °C. Table 4. THERMOFLOW® software simulates the necessary total cooling load by using the energy balance formula:[6]

$$Q_{CL} = m_{air}\,[(h_a - h_c) - hf_{g,c}\,(\omega_a - \omega_c)][6] \quad (1)$$

Description	Unit	Value
Air mass flow rate to be cooled at GT inlet (M_a)	Kg/s	115
Air temperature – site condition – RH = 70 %	°C	32
Enthalpy – Inlet air - h_a	kJ/kg	86.26
Air temperature after coil	°C	15
Enthalpy – air after cooling - RH = 100 % - h_c	kJ/kg	42.20
Heat to be removed per machine - Q_{CL}	kW	4.560
Heat to be removed per machine - Q_{CL}	TR	1.420
Total heat to be removed - 2 machines	TR	2.800

Table 1. Absorption chiller-dimensioning

Chilled water capacity THERMOFLOW® simulation based on heat transfer formula:

$$Q_{cw} = M_{cw} * Cp_{cw} * (T_{cw2} - T_{cw1})\ [6] \quad (2)$$

Description	Unit	Value
Mass flow rate for 1 TR	Kg/s	0.139
Vol flow for 1.420 TR + 10%	M^3/h	752
Total Vol flow – 2 machines	M^3/h	1.500

Table 2. Chilled water capacity [5]

3. GT - EXTRA POWER CALCULATION & ECONOMIC ANALYSIS & RESULTS

The AC needs a constant (4.2 bar) low-pressure steam, with a mass flow rate of 3.5 kg/s (4.5kg/h-RT) in accordance with AC manufacturer specs. THERMOFLOW® software simulation indicates that the ST power output decreases by around 1.82 MW. This is a very conservative calculation. Table 3. LCC evaluation results.

Premises & LCC Evaluation Results		
Interest rate - Brazil		15 %
Currency exchange rate - Real /US$	08/01/2017	3,11
MWH Price - Rio de Janeiro + taxes	ANEEL – R$ 628,00	$201.58
Life time service	Years	20
ST losses + Auxiliary electric load	MWH per/year	17.243
TIC capital cost		$14,700.000
GT system availability record		95 %
TIC system O&M cost	Per year	$965,000
CCPP extra power delivered	Per year	69.248
Net Present Value (NPV)		$67,263.511
Payback period	Year	1.5

Table 3. LCC evaluation results

4. CONCLUSIONS

The TIC - turbine inlet air-cooling system application is feasible and very attractive. Nowadays, the AC – absorption chiller technology can be considered as a reliable alternative with several successful applications worldwide.

The estimated net electric power production would increase by 69.248MWh/yr. The payback period is 1.5 years, and the net present value (NPV) is 67.26 MUS$.

5. REFERENCES

[1] Doom, T. R., 2013. “Case studies on the government’s role in energy technology innovation – Aeroderivative Gas Turbines”.

[2] Kurz, R., 2005. “Gas turbine performance”. In Thirty-fourth Turbomachinery Symposium. San Diego, California, USA.

Preparation of N-Functionalized Graphitic Carbon by Catalyst-Free Pyrolysis of the Biomass Wastes Chitosan and Chitin

Author: Thatiana Crispim da Silva[1], José Carlos Netto-Ferreira[2], Eric Cardona Romani[3], Suzana Bottega Peripolli [4], Rachel Novaes Gomes[5,6], Paula Dias Barboza[5,6], Sergio Noboru Kuriyama[5,6], Cecília Vilani[7], Juan Lucas Naches[8], José Brant de Campos[1], Antonio Augusto Fidalgo Neto[5,6#]

[1] Programa de Pós-Graduação em Engenharia Mecânica – PPG-EM, Universidade do Estado do Rio de Janeiro, Brazil; [2]Departamento de Química, Universidade Federal Rural do Rio de Janeiro, Brazil; [3] Instituto SENAI de Inovação em Sistemas Virtuais de Produção, Sistema Firjan, RJ, Brazil ; [4] Instituto SENAI de Tecnologia Solda, Sistema Firjan, RJ, Brazil; [5] **Centro de Inovação SESI em Higiene Ocupacional, Sistema Firjan, RJ, Brazil**; [6] Instituto SENAI de Inovação Química Verde, Sistema Firjan, RJ, Brazil. ; [7]Departamento de Engenharia Química e de Materiais, Pontifícia Universidade Católica do Rio de Janeiro, RJ, Brazil; [8] Centro de Pesquisas Gerais, Universidade Federal Fluminense, Brazil.

PPG-EM Seminars: season **2017**
www.ppg-em.uerj.br

July 18, 2016

Keywords: Chitin, Chitosan, Adsorption, Formaldehyde.

1 Introduction

Formaldehyde (FA) is a volatile organic compound considered one of the largest pollutants in indoor environment. Of predominant anthropogenic origin, it is a major irritant to the eyes and pharynx. However, the major concern of FA exposure is related to IARC classification on group 1 – carcinogenic to humans - which raised great public awareness. In this context, developing a new material for FA adsorption has a global interest due to the large industrial use in several segments. Therefore, here we propose the use of a new carbonaceous material containing Nitrogen derived from the biomass wastes Chitosan and Chitin for the detection and adsorption of formaldehyde. Favorable carbonyl–adsorbent interaction in the case of formaldehyde can be expected due to the presence of the N-functionalized graphitic carbon. Following green chemistry principles, avoiding any unfriendly metal catalyst and using a single carbon and nitrogen source from inexpensive biomass wastes, graphitic carbons were produced upon pyrolysis of chitosan and chitin at 700 °C.

2 Methodology

The synthesis of the graphitic carbons was carried out at 700 °C using either chitosan or chitin as a carbon source. In a typical synthesis, 1.00 g of chitosan or chitin was heat-treated in a furnace, under air, at 700 °C with a ramp time of 5 °C / min. Microelemental analysis was performed with a Vario Micro cube elemental analyzer. Raman spectroscopy was performed with WITec and using a 532 nm laser excitation source. X-Ray Diffraction was performed with a PANalytical X'Pert diffractometer using a angular detector.

Formaldehyde was detected and quantified as described by the NIOSH FORMALDEHYDE: METHOD 2016, Issue 2, 2003.

3 Results

Elemental analysis (tab. 1) shows that with the pyrolyzed material there is an increase in the amount of nitrogen present. Raman spectroscopy results with peaks at 1400 and 1600 show that the material is carbonaceous (Fig. 1). Finally, the results of X-ray diffraction reveal the phase change that occurs after pyrolysis. Chitosan that had an amorphous and nanocrystalline phases, after pyrolysis has amorphous, crystalline phases. However, the chitin that before the pyrolysis had basically crystalline phases, after the pyrolysis process shows amorphous, nanocrystalline and crystalline phases (fig.2).

Sample	Weight (mg)	N [%]	C [%]	H [%]	O [%]
Chitosan	1.937	7.67	40.92	7.44	43.96
Chitosan T700	2.059	11.22	76.03	3.04	9.71
Chitin	1.896	7.21	42.73	7.66	57.60
Chitin T700	2.028	10.49	76.11	2.97	10.42

Table 1 – Elemental analysis: Chitosan, chitin and pyrolyzed samples at 700 ° C.

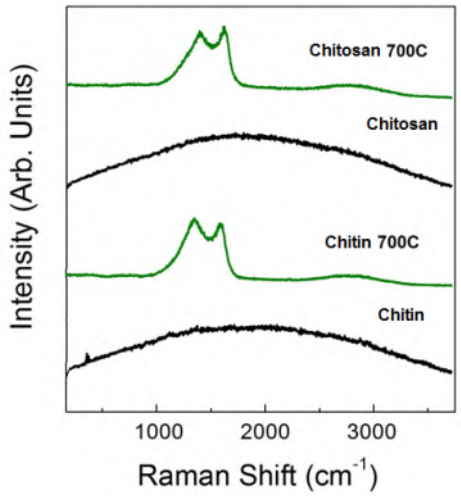

Fig.1 – Raman spectra of commercial chitin and chitosan and pyrolysed at 700°C. Spectra were obtained using a Raman spectrometer with a 532 nm laser excitation source.

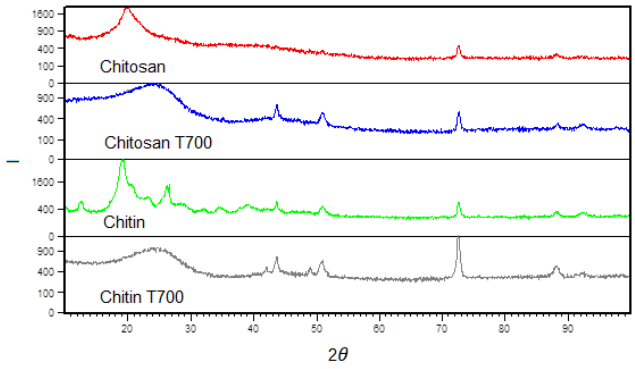

Fig. 2 – X-ray diffraction results of commercial chitin and chitosan and pyrolyzed at 700°C.

For the adsorption test, a formaldehyde concentration of 25ppm was generated in the adsorption system (chamber of 5,35 L). Forty milligram of pyrolyzed (700°C) chitosan or chitin were submitted to a flow of 500 cc/min during 1h (fig.3). After that, the remaining gaseous FA was evaluated and expressed as % of FA removed (tab. 2).

Sample	Amount of adsorbed formaldehyde (%)
Chitin T700	28,8
Chitosan T700	41,6

Table 2 – Adsorption data for formaldehyde

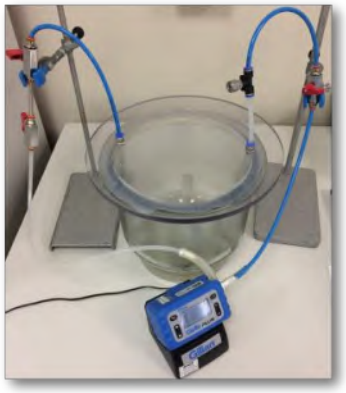

Fig. 3 – Adsorpsion test system

4 Conclusions

In conclusion, pyrolysis of the biomass wastes chitin and chitosan at 700 °C led to the formation of carbon materials which were characterized by Elemental Analysis, FTIR and Raman Spectroscopy and X-ray diffraction. From the later, the carbon material structures clearly show crystalline, nanocrystalline and amorphous phases. The preliminary results of the adsorption experiments confirm that formaldehyde can be efficiently adsorbed on these materials and could be used as a possible alternative for adsorption of formaldehyde in the occupational environment.

References

[1] Primo, A., Forneli, A., Corma, A., Garcia, H. ChemSusChem, 2012, 5, 2207.

[2] Primo, A., Atienzar, P., Sanchez, E., Delgado, J. M., Garcia, H. Chem. Comm., 2012, 48, 9254.

[3] Olejniczak, A., Lezanska, M., Wloch, J., Kucinska, J., Lukaszewicz, P., J. Mater. Chem. A, 2013, 1, 8961.

[4] Lezánskaa, M., Olejniczaka, A. Pacułac, A., Szymánskia, G., Włoch, J., Cat. Today 2014, 227, 223.

[5]Xia, Y., Yang, Z., Mokaya, R., Nanoscale, 2010, 2, 639.

ANALYSIS OF THE MICROCLIMATE OF SÃO CRISTÓVÃO AND ITS INFLUENCE IN HEATING SYSTEMS, VENTILATING AND AIR CONDITIONING (HVAC)

Author: Marcelo Fernandes Melo Monteiro[1] *marcelofmm@gmail.com*
Advisor: Manoel Antônio da Fonseca Costa Filho[1]

[1] State University of Rio de Janeiro

PPG-EM Seminars: season **2017**
July 19, 2017 www.ppg-em.uerj.br

Keywords: Heating, Ventilation, Air-Conditioning and Weather data.

1 Introduction

The metropolitan region of Rio de Janeiro has a high population density and a very high degree of industrialization, and as a consequence a large concentration of pollutant emissions and heat sources. Its topographic and atmospheric peculiarities directly affect the dispersion of air pollutants and heat. Furthermore, the land use characteristics of the region with a high percentage of areas covered with asphalt and concrete are able to convert and store solar radiation into a greater extent than rural areas, promoting the onset of a horizontal temperature gradient phenomenon known as the urban heat island [1].

This manuscript aims to investigate the influence of urban microclimate on air conditioning designs through using climatic data from the closest meteorological station instead of those recommended by the Brazilian air conditioning design standard ABNT NBR16401. For the city of Rio de Janeiro, this standard provides climatic data from Antônio Carlos Jobim International and Santos Dumont Airports. Both are located next to the sea, so it can be supposed that they are less impacted by the urban heating.

2 Materials and Methods

The building has an area of 120m² and it is internally divided into administrative room, reception, security room, circulation area, information technology room, dining room and bathrooms. It is placed in the Sao Cristovao neighborhood, and for this investigation, strategically located where there is a meteorological station. Sao Cristovao is far respectively, 6 km and 10 km, from the Santos Dumont and Antonio Carlos Jobim airports. These distances were approximately measured through straight lines using a specific tool available in the Google Maps (figure 1). For any place in the Rio de Janeiro city, there is no indication in the NBR 16401 about what climatic data must be chosen. It is well known that air conditioning designers adopt the highest temperature data.

The São Cristóvão meteorological station belongs to the Fundação Instituto de Geotécnica (Geo-Rio), within the Rio de Janeiro's City Hall, a department created for monitoring the rainfall in order to warn the population about risks of slope slips. It is located at the latitude of -22.896667, the longitude of -43.221667 and an elevation of 25 meters, on the top of the Geo-Rio building. This station measures and records temperature, humidity, pressure, rainfall and wind speed at 15 minutes intervals. It has supplied access to download data since 2002, but the period used here is from 2003 to 2015 [2].

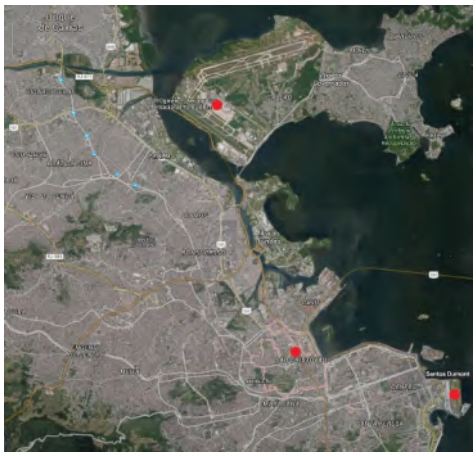

Figure 1. Location of weather stations (Google Maps)

São Cristóvão climatic data must be processed following a methodology defined by ASHRAE (2013) in order to generate a climatic data table similar to those available in the NBR 16401. It requires an extensive database obtained by direct measurement of several variables, hourly, over a period of at least eight. Among the data required is the design temperature, which for conventional cooling designs is the dry bulb temperature (DBT). This is achieved by arranging the data stored in the measurement frequency vectors, and calculating the temperature which is only equaled or exceeded by a specific percentage of the total number of times of the year. The percentages

correspond to desired frequency levels. The coincident wet bulb temperature (CWBT) is obtained by arranging the stored data in frequency matrices by averaging the wet bulb temperatures that occur along with the calculated DBT [3].

The dry bulb temperature, dew point (DPT) and wet bulb temperature and wind speed corresponding to different annual percentage representing the value that is exceeded on average by the percentage indicated the total number of hours per year (8760h). The 0.4%, 1.0% and 2.0% are exceeded, on average, 35h, 88h, 175h per year, respectively, for the record period [3].

Meteorological data sets used for the calculations may contain missing values. Gaps up to 6 hours were filled by linear interpolation to provide the most complete possible time series. When the data at the right time are lacking, they can be replaced by data up to 0.5 hours before or after, when available [3].

Some months were also eliminated during the additional quality control checks. The dry bulb temperature of a station will only be used for design calculation if there was data from at least eight months that met the quality control and selection criteria from the registration period for each month of the year [3].

Microsoft Excel was used for data processing. Downloaded climatic data are formatted with columns corresponding to climatic variables and lines to time. Only DBT, relative humidity and pressure columns were maintained, all other columns were deleted. Then, the lines corresponding to fifteen, thirty and forty five minutes were also eliminated. The lacking of DBT data was searched, and when found, data were fulfilled with the closest available, within a thirty minute interval. So, DBT data were arranged in ascending order to find the DBTs that correspond to the frequency levels of 0.4%, 1.0% and 2.0%. Finally, the coincident relative humidity and pressure values were determined as the average ones. CWBT and DPT were read in a psychrometric chart.

3 Results

The DBT for São Cristóvão was approximately a mean value between the others, accomplishing its geographical location. On the other hand, both CWBT and DBT for São Cristóvão were the lowest for all frequency levels. This was expected since São Cristóvão is more far from the sea than other stations. Table 1 presents DBT, CWBT and DPT at the three frequency levels for the Santos Dumont and Antônio Carlos Jobim airports and São Cristóvão.

Frequency Level	T[ºC]	São Cristóvão	Santos Dumont	Antônio Jobim
0.40%	DBT	36.2	34.0	38.1
	CWBT	24.0	25.2	25.6
	DPT	19.0	25.3	27.1
1.0%	DBT	34.5	32.7	36.2
	CWBT	24.1	25.0	25.3
	DPT	19.9	25.0	26.2
2.0%	DBT	33.2	31.8	35.0
	CWBT	23.6	24.9	25.2
	DPT	19.7	24.6	26.0

Table 1. Thermal Load

After defined the entry temperatures, thermal load calculations were made in order to evaluate their influence on the air conditioning design. Graphic 1 shows the thermal loads corresponding to the three places at the three frequency levels, with a vertical bar representation illustrated in Figure 6. The Antônio Carlos Jobim airport had the highest thermal load at all frequency levels. The thermal loads for São Cristóvão and Santos Dumont airport are very close at the frequency levels of 0.4% and 1.0%.

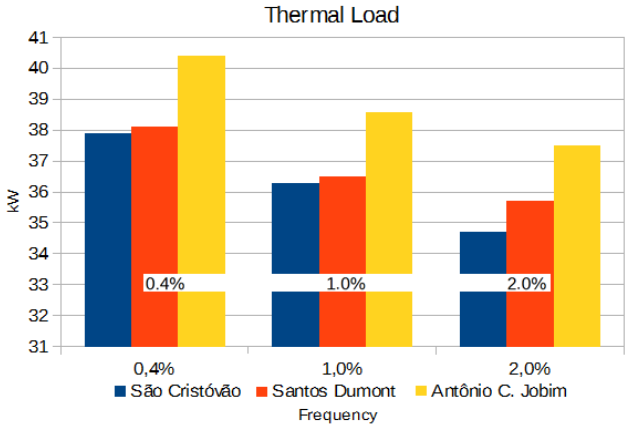

Graphic 1. Thermal Load

4 Conclusions

The DBTs calculated for São Cristóvão have confirmed that there is an increasing temperature gradient from the south to the north in the study region. Since São Cristóvão is a neighborhood where buildings up to 2 floors are predominant, the elevation of its meteorological station has contributed to a negligible urban heating perception.

Although the DBT for São Cristóvão is midway between the others, the thermal load for São Cristóvão was the lowest. This can be justified due to its lower air humidity.

The variations of the thermal loads among the sites chosen are around 6% for the studied construction, which does not significantly interfere in the selection of the air conditioning equipment. At first the size of the building should be higher for that percentage has a significant impact on thermal load calculation.

References

[1] R. B. Stull. *An Introduction to Boundary Layer Meteorology*. Kluwer Academic Publishers, 1993.

[2] Sistema de Alerta Rio da Prefeitura do Rio de Janeiro, ALERTA RIO, *http://alertario.rio.rj.gov.br/*, Rio de Janeiro - RJ, 2016.

[3] American Society of Heating, Refrigerating, and Air-Conditioning Engineers. *Climatic Design Information*. Handbook Fundamentals, ASHRAE, Atlanta - GA, 2013.

ANALYSIS OF HEAT INTERACTION BETWEEN FINS AND VARIABLE THERMAL CONDUCTIVITY

Author: Jonatas Motta Quirino[1] *quirinojm@hotmail.com*
Advisors: Eduardo Dias Corrêa[1] ; Rodolfo do Lago Sobral[2]
[1] State University of Rio de Janeiro
[2] Federal Center of Technological Education

PPG-EM Seminars: season **2016**
www.ppg-em.uerj.br
Oct 25, 2017

Keywords: Extended surface, Heat dissipation, Thermal radiation, Mutual effect.

1 Introduction

The present work describes the thermal profile of a fin, which dissipates heat. Neumann and Dirichlet boundary conditions are established. Heat transfer analysis is performed by computational simulations. The Finite Differences Method is applied to the problem formulation. The thermal conductivity is as a function of temperature. Double fins are analyzed, where their surfaces interact thermally, generating mutual effects. Finally, the comparison of the results proves that the assumptions of variable thermal conductivity, heat dissipation by thermal radiation and mutual interaction are crucial to obtain results that are closer to reality.

2 Definitions and descriptions

The Fig. 1 presents a *Single Fin* which has only one surface extended to the primary surface and *Double Fin* which has two extended surfaces to the primary surface, where the distance between them is very small.

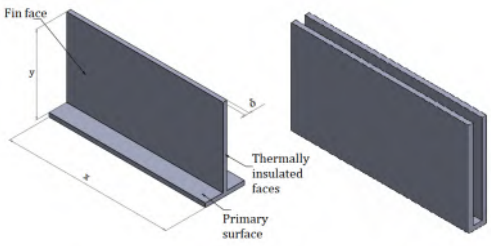

Figure 1: Fins

Some considerations should be made: The thermal transient is neglected; The fin is not a source of its own heat; and the double-fins have exactly the same geometric dimensions and are positioned symmetrically.

3 Mathematical approach

As one of the definitions of the problem is the condition of thermal steady state, the thermal distribution in the directions of each Cartesian axis of the fin, is [4]

$$\frac{\partial}{\partial x}\left(k(T)\frac{\partial T}{\partial x}\right)+\frac{\partial}{\partial y}\left(k(T)\frac{\partial T}{\partial y}\right)+\frac{\partial}{\partial z}\left(k(T)\frac{\partial T}{\partial z}\right)=0 \quad (1)$$

By the definitions of fins, only in the axis y the temperature differences between their points are considerable. This formulation suggests that the problem is analyzed in a one-dimensional approach.

3.1 Boundary conditions

Two mathematical boundary conditions (b.c.) were used. These conditions are very common in mathematical problems involving differential equations, as shown in Fig. 2.

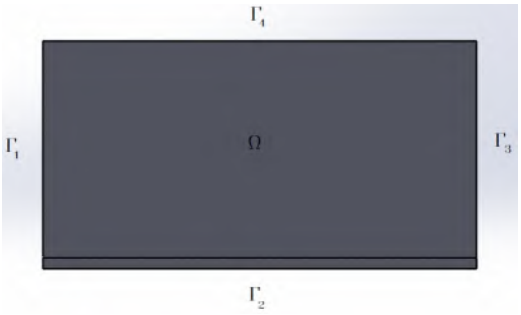

Figure 2: Boundary and domain

- The faces Γ_1 $(x = 0)$, Γ_3 $(x = L)$ and Γ_4 are thermally isolated. (Neumann b.c.)
- The face Γ_2 $(y = 0)$ is conditioned with a certain temperature imposed on it. (Dirichlet b.c.)
- In the faces $z = 0$ e $z = \delta$, heat dissipation is considered by thermal convection and radiation.

3.2 Application to modeling

Based on the assumptions and the boundary conditions presented, it follows that [3]:

$$\frac{d}{dz}\left(k\frac{d\overline{T}}{dz}\right) = -\frac{2}{\delta}[h\left(\overline{T} - T_\infty\right) + \varepsilon\sigma T^4] \qquad (2)$$

Where k will be treated as a variable in function of y.

The mathematical result of the interaction between the fins in a radiation-only perspective is given by the following integral [5]:

$$E_{mut} = \int_0^b \sigma\overline{T}^4(\xi)\left(\frac{d^2}{2[(y-\xi)^2 + d^2]^{\frac{3}{2}}}\right)d\xi \qquad (3)$$

3.3 Numerical methods

For the characterization of the thermal conductivity profile, it is necessary to trace parameters that relate the thermal conductivity (k) and temperature (T).

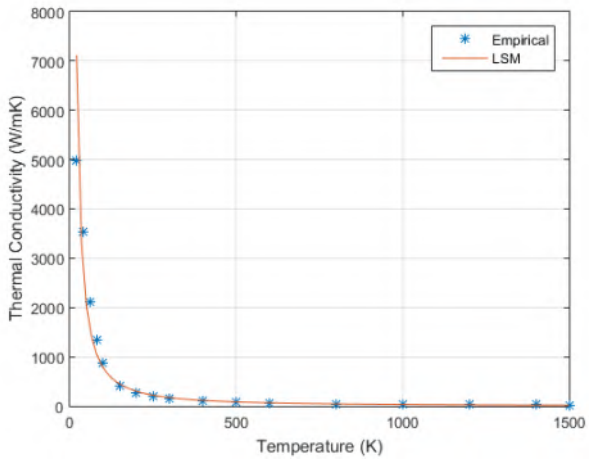

Figure 3: Curve fitting by LSM in exponential type

The method used was the *Least Squares Method* (LSM), where the empirical data were stipulated [1] and the approximation is illustrated in Fig.3.

In order to solve numerically the partial derivatives present in the problem studied, is used the Finite Differences Method(FDM). [2]

Given these relations, after algebraic adjustments takes the following form.

$$T_j = \frac{\delta}{2k_j + 2hl^2}\left[T_{j+1}\left(\frac{k_j - k_{j-1}}{2} + k_j\right) - T_{j-1}\left(\frac{k_j - k_{j-1}}{2} - k_j\right)\right] + \frac{2hl^2T_\infty}{2k_j + 2hl^2} - \frac{2\varepsilon\sigma T_{rad}}{2k_j + 2hl^2} \qquad (4)$$

4 Results and conclusions

A graph in Fig.4 was generated that overlapped all the results in order to demonstrate the discrepancy between the results in all situations analyzed.

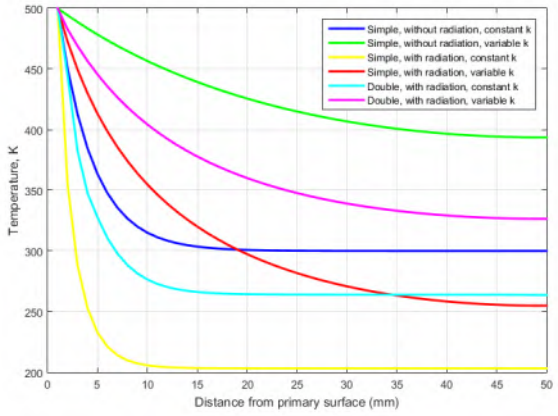

Figure 4: Comparison of generated thermal profiles

In this study, it was noted the importance of evaluating commonly overlooked phenomena, which generate very considerable discrepancies to the final results. The errors related to the expected result reached maximum values of 49.84%.

It can be concluded, therefore, that thermal dissipation analysis, in order to approach a real model, should never neglect the variation of thermal conductivity, the effects of thermal radiation and mutual interaction.

5 Acknowledgments

The author thanks all teachers, advisors, UERJ for the support and to CAPES for the funding of the study.

References

[1] Cho Yen Ho, Reginald W Powell, and Peter E Liley. Thermal conductivity of the elements. *Journal of Physical and Chemical Reference Data*, 1(2):279–421, 1972.

[2] Jack Philip Holman. *Heat transfer*. McGraw-Hill, 2010.

[3] Allan D Kraus, Abdul Aziz, and James Welty. *Extended surface heat transfer*. John Wiley & Sons, 2002.

[4] Alfio Quarteroni, Riccardo Sacco, and Fausto Saleri. *Numerical mathematics*, volume 37. Springer Science & Business Media, 2010.

[5] Rodolfo do lago Sobral. *Simulação numérica de aletas num contexto de altas temperaturas*. PhD thesis, Universidade do Estado do Rio de Janeiro, 2017.

INFLUENCE OF DISPERSION OF GRAPHENE OXIDE AND REDUCED GRAPHENE OXIDE ON POLYURETHANE IN GAS PERMEATION

Author: Alessandro Eronides de Lima Silva[1] *alessandroero@gmail.com*
Advisor(s): José Brant[1]
[1] State University of Rio de Janeiro

PPG-EM Seminars: season **2017**
November 08, 2017 www.ppg-em.uerj.br

Keywords: graphene diperson, gas permeation, polyurethane.

1 Introduction

Polymer nanocomposites have attracted great interest both in academic and industrial terms, due to the potential for significant increase of properties obtained with small amounts of nanoparticles added to the polymer matrix [2]. The graphene oxide, combined with polymers, has shown an impermeable nanocomposite barrier to gases and liquids [5] and from this perspective it has attracted a particular interest for applications on oil and gas industry. In many cases, nanocoating acts as protective film that may prevent future corrosion problems [1] and extend the devices lifetime. In this work, we use ultrasonic Tip to increase the dispersion of graphene oxide (GO) and reduced graphene oxide (RGO) on polyurethane compared to using only magnetic stirrer. The samples obtained have been tested in a permeation analysis system. Friction measurements were taken using a micro-tribometer in a ball-on-flat contact geometry with a stainless steel ball as the counterbody. The coating films were studied by scanning electron microscopy (SEM), optical microscopy, atomic force microscopy (AFM) and Raman Spectroscopy.

2 Experimetal

The manufacturing process of the samples occurred as follows: first the polyurethane and solvent THF (tetrahydrofuran) are left in magnetic stirring for 24 hours, then is added the Graphene (GO or RGO) used in ultrasonic tip and left for another 24 hours in magnetic agitation before being spread on a camera in THF saturated for the membrane formation. After the formation of the membranes, they were tested in the permeation system and friction behavior.

The Raman spectrum obtained on the samples with GO and RGO proved the presence of graphene in both [3]. The figure 1 shows the Raman spectrum obtained on the sample with GO and the figure 2 shows the sample with RGO.

The permeation system consists of a cell fed by a gas (CO2) at constant pressure, the membrane is placed inside the cell to hinder the passage of gas. After the membrane is attached a pressure transducer. As the pressure increases on the transducer and these data are acquired for a computer, it is possible to correlate the pressure curve obtained with the tested membrane permeability.

The friction behavior test were conducted using a micro-tribometer CTER-UMT under linear reciprocating sliding configuration performed at constant load 1 N to access the friction coefficient. [4]

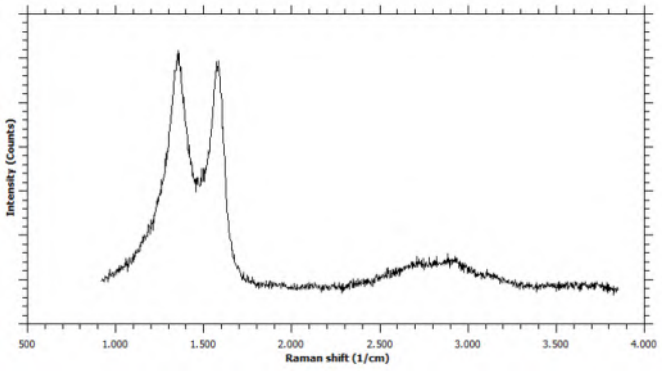

Figure 1: Spectrum Raman GO/PU nanocomposite

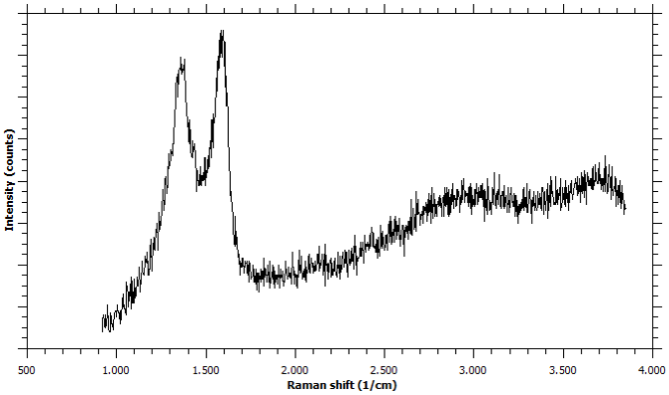

Figure 2: Spectrum Raman RGO/PU nanocomposite

3 Results

The analysis of Graphene dispersion by different methods of manufacture of samples can be evaluated. Figure 3 shows the characterizations made by optical microscope samples of GO/PU (a) and RGO/PU (c) without using the tip, in comparison with the samples GO/PU (b) and RGO/PU (d) using the ultrasonic tip.

SEM microscope was used to obtain a greater magnification on the flake of Graphene. Figure 4 (a) shows the cluster of GO in the sample that has not been used the ultrasonic tip. While Figure 4 (b) shows the Graphene better dispersed in the sample who used the ultrasonic tip.

The analysis of the morphology of the surface was performed through the AFM. Figure 5 shows the morphology of samples (a) GO/PU and (b) RGO/PU both manufactured with the use of the ultrasonic tip.

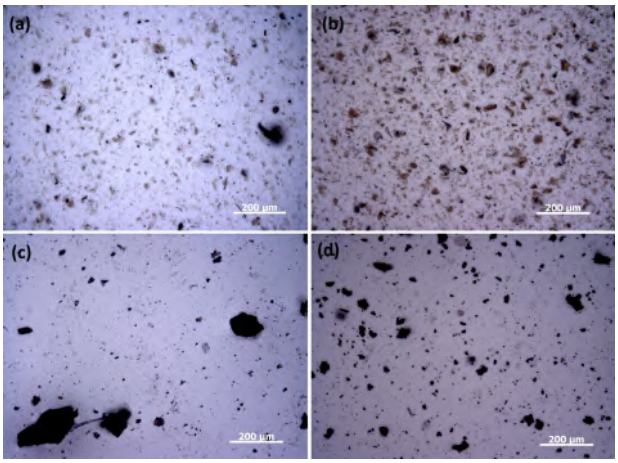

Figure 3: Optical microscope images. (a) GO/PU without using Ultrasonic tip, (b) GO/PU using ultrasonic tip, (c) RGO/PU without using Ultrasonic tip, (d) RGO/PU using ultrasonic tip.

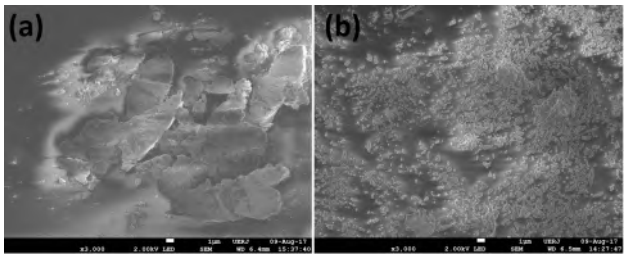

Figure 4: SEM microscope images. (a) GO/PU without using Ultrasonic tip, (b) GO/PU using ultrasonic tip

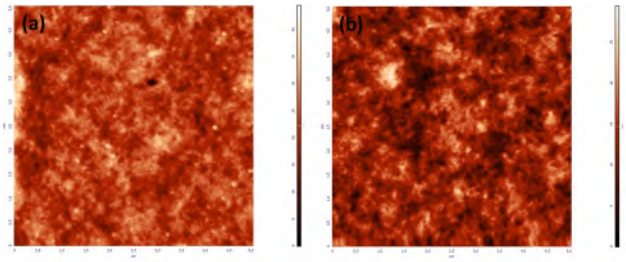

Figure 5: AFM microscope images. (a) GO/PU without using Ultrasonic tip, (b) GO/PU using ultrasonic tip

4 Conclusions

After the analysis of the optical microscope images it is possible to affirm a better dispersion of the flakes of Graphene from samples of GO and RGO who used the ultrasonic tip in your manufacturing, in comparison with the samples that were manufactured only by magnetic stirring. The observation of the flakes to GO in greater magnification, through the SEM, can check a better distribution of the sample used the ultrasonic tip. AFM images revealed no significant differences in morphology between the samples examined. In this way, it can be concluded:

- ultrasonic probe in manufacturing of membranes improved Graphene dispersion in polyurethane;
- It is Expected a better performance of the samples using the ultrasonic tip for permeation test, once a more homogeneous dispersion of the Graphene contributes to improving the barrier against gas passage in these membranes;

5 Acknowledgments

The author thanks the Van Der Graff Laboratory of the physics department at PUC-Rio for giving a structure for the development of the research and all the support.

References

[1] R. Asmatulu. Nanocoatings for corrosion protection of aerospace alloys. 2012.

[2] Yanbin Cui, S.I. Kundalwal, and S.Kumaraca. Gas barrier performance of graphene/polymer nanocomposites.

[3] A. C. Ferrari, J. C. Meyer, V. Scardaci, C. Casiraghi, M. Lazzeri, F. Mauri, S. Piscanec, D. Jiang, K. S. Novoselov, S. Roth, , and A. K. Geim. Raman spectrum of graphene and graphene layers. 2006.

[4] E. C. Romani, D. G. Larrude, L. Nachez, C. Vilani, J. B. de Campos, S. B. Peripolli5, and F. L. Freire Jr. Graphene grown by chemical vapour deposition on steel substrates: Friction behaviour. 2017.

[5] S.C.Tjong. Structural and mechanical properties of polymer nanocomposites. 2006.

CHARACTERIZATION OF JOINT WELDED BY TUNGSTEN INERT GAS (TIG) AUTOGENOUS STEEL PROCESS UNS S32707 SIMULATING A HEAT EXCHANGER FOR OIL HEATING

Author: Waleska Gonçalves[1] *wal.goncalves1@gmail.com*
Advisor(s): Marília Garcia Diniz[1]
[1] State University of Rio de Janeiro

PPG-EM Seminars: season **2017**
www.ppg-em.uerj.br
November 15, 2017

Keywords: hyper duplex, TIG welding, nitrogen

1 Introduction

The hyper duplex steels have a biphasic structure, in the same proportion of austenite and ferrite. They are widely used because they have excellent mechanical properties and great resistance to corrosion in aggressive environments, such as in deep water and heat exchangers, in oil refineries. The study of this material is important because with its welding there is the possibility of the formation of undesired phases which would decrease the high resistance desired to it, so it is very important that it present its biphasic equilibrium under any circumstances. For this phase equilibrium to be maintained, chemical stabilization elements in each phase must be included. The inclusion of nitrogen is used to stabilize the austenitic phase and the ferrite phase is stabilized by the chromium element. [2] In welding TIG autogenous, which is the focus of this work, the biggest problems occur with the increased presence of ferrite, the formation of chromium nitride and the presence of deleterious phases such as sigma or chi which to cause increased hardness in the material, that do the corrosion resistance worsens. With the addition of nitrogen to the shielding gas, together with the argon, the austenite is not lost with the formation of the base metal.

This study analyzes the welding joints of hyper duplex steel UNS S32707 with two different amounts of nitrogen present in the protective gas, with the highest value being 5.5% in relation to the amount considered standard by the industry of 2.5% in the TIG welding process by measuring hardness profiles and SEM, EDS and EBSD techniques. There is also a study of the corrosion resistance of these welded joints through the mass loss corrosion test according to standard ASTM G-48 simulation working conditions of heat exchangers in oil refineries, where crude oil at high temperature is used.

2 Methodology

The base metal is a hyper duplex steel UNS S32707 type with biphasic austenitic-ferritic microstructure. The Autogenous TIG welding its purpose to simulate a pipe sealing conditions in heat exchanger. They have no addition metal and the sample as in seamless pipes, annealed.

Two samples with different percentages of nitrogen in the protection gas composition were studied. One with 2.5%, as usually used commercially and with 5.5%, considered an acceptable value for the phases to remain as in their original biphasic state. The Vickers (HV) microhardness measurements on welded joints tested was performed to determine if there have any variation in the mechanical properties of the samples between the critical regions: the base metal (BM) and fusion zone (FZ). The part of analysis microscopy was performed in SEM (Scanning Electron Microscope) and was realized to determine the present phases in the microstructure and for the possible to encounter possible undesirable precipitates. They occurred in two stages: one with low increase (up to 1000X) and large increase, respectively. The EDS (X-Ray Energy Dispersive Spectroscopy) is used for semiquantitative analysis of the chemical elements present in the samples. The Vickers microhardness and the analysis in microscopy was done together with the doctoral thesis of André Pimenta. [3]

The technique of EBSD (Electron Backscatter Diffraction) allows the determination of orientations and phase compositions of any plane or crystallographic direction. The corrosion testing with working fluid (crude oil) are performed according to ASTM G48 – 99 [1] method A - mass loss corrosion test in working temperature of 220 °C. For established this temperature, a study was realized with a schematic of the petroleum distillation line and was chosen the worst scenario.

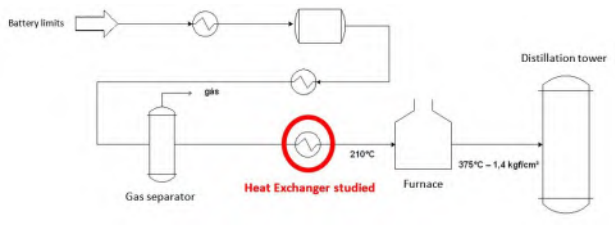

Figure 1: Schematic of the petroleum distillation line. The heat exchanger is located in the indicated area. Working temperature is 210 °C.

3 Results

The Vickers microhardness measurement profile of the two samples is in a very similar range between them, with no differences. This proves that the inclusion of nitrogen in the base metal did not leave the sample fragile as expected. SEM results show well delimited ferrite and austenite phases for the two samples in the heat affected zone and do not present undesired precipitates as nitrides. The EDS was performed in both phases. No stranger elements were found in the original alloy, so there is no contamination of the metal base or welding process. In the EBSD results, two different techniques were applied: the SEM analysis and the phase compositions, shown in figures 4 and 5 respectively. Two different regions are indicated, one non-welded and welded. As well as the SEM result, the phases are well delimited and the percentage is very close in the biphasic microstructure.

SEM results:

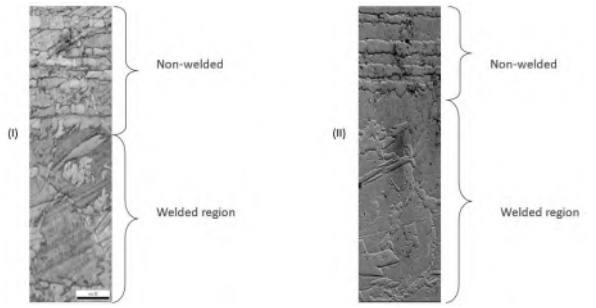

Figure 2: Comparison of the two welded regions together with the base metal (I) standard sample composed of 1.5% N; (II) modified sample composed of 5.5 % of N

Phase Composition:

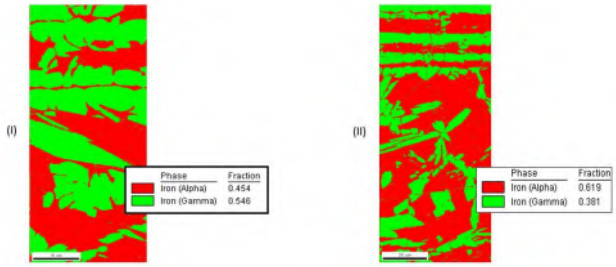

Figure 3: Comparison with respect to the composition of Ferrite (Red) and Austenite (Green) phases, with their percentages. (I) standard sample composed of 1.5 % N; (II) modified sample composed of 5.5% of N.

The corrosion test with the crude oil indicated good results showing no mass loss in high temperature. the corrosion test commonly performed for stainless steels (according to ASTM G 48 - method A and temperature effect) was not adequate to evaluate differences in corrosion resistance between the different types of welded samples, since the results obtained were not consistent.

4 Conclusions

- Tests with the SEM and EDS have confirmed that addition of the amount of nitrogen in the shielding gas causes the amount of austenite to stabilize in the fusion zone. This proving what the literature indicates that the hyper duplex steel has a better resistance to corrosion ;
- The EBSD technique the test proved to be very effective and could be further explored and still used in other studies;
- The corrosion test of the type indicated in ASTM G 48 - method A, chosen for this study and carried out in the laboratory, did not indicate precise results and it is necessary to perform other types of corrosive tests for more conclusive results;

References

[1] ASTM. Standard test methods for pitting and crevice corrosion resistance of stainless steels and related alloys by use of ferric chloride solution. AMERICAN SOCIETY FOR TESTING AND MATERIALS, 1999.

[2] G.; Kangas P. Chail. Super and hyper duplex stainless steels: structure, proprieties and applications. *Procedia Structural Integrity*, 2:1755–1762, 2016.

[3] A. Pimenta. *Análise da influência de elemento estabilizador da austenita em aço inoxidável hiperduplex UNS S32707 soldado por processo TIG.* Tese de doutorado, Universidade do Estado do Rio de Janeiro, Rio de Janeiro - RJ, 2016.

PREPARATION OF GRAPHITIC CARBON BY CATALYST-FREE PYROLYSIS OF LIGNIN TO REDUCE VOLATILE ORGANIC COMPOUND OF THE WORK ENVIRONMENT

Author: Sérgio Leandro Soares Itajahy Pinto da Costa[1] *leandroatalaia@poli.ufrj.br*
Advisor(s): José Brant de Campos and Suzana Bottega Peripolli [1]
[1] State University of Rio de Janeiro

PPG-EM Seminars: season **2017**
November 22, 2017 www.ppg-em.uerj.br

Keywords: Lignin, Pyrolysis, Adsorption.

1 Introduction

In the last decades the chemical industry has intensified its efforts to reduce, prevent and eliminate the environmental impacts. At the same time, there is a growing concern for human well-being. Monitoring the work environment is increasingly common, thus ensuring the safety and health of the worker. Emissions of volatile organic compounds have motivated several research activities to develop efficient and low cost technologies for their capture. The preparation of a carbonaceous material from lignin, the second most abundant biopolymer in the nature and sub product of the paper industry, appears as an alternative to this demand. Mesoporous graphitic materials can be obtained from lignin pyrolysis at 800°C and deposited in polymer matrices or quartz plates for the physical adsorption of these harmful substances thus a filter is created to prevent diseases and ills caused by VOC's and the most important, using an industrial waste[1, 2].

2 Methodology

The synthesis of the graphitic carbons was carried out at 800°C using Lignin as a carbon source. In a typical synthesis, 2.00g of Lignin was heat-treated in a furnace, under air, at 800°C with a heating rate of 5°C/min. Fourier-Transform Infrared Spectroscopy (FTIR) was performed with a Varian 600 FTIR spectrometer with the number of scan times of 256 as showed in Figs. 1 and 2. Raman spectroscopy was performed with WITec and using a 532nm laser excitation source. X-Ray Diffraction was performed with a PANalytical X'Pert diffractometer using a angular detector. Formaldehyde quantification followed the method NIOSH Manual of Analytical Methods (NMAM), with high performance liquid chromatography with UV detector (HPLC-DAD).

3 Results

This section shows the experiments results before and after pyrolysis, exhibiting differences in the morphology like crystallinity, present phases and changes in the nanostructures.

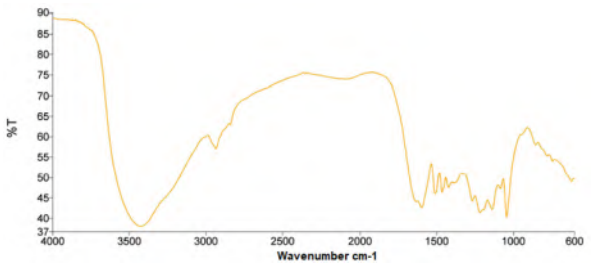

Figure 1: FTIR spectra of commercial Lignin as received.

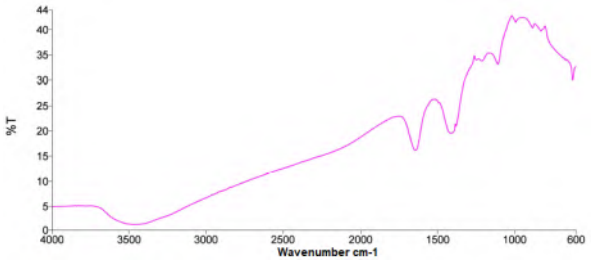

Figure 2: FTIR spectra of commercial Lignin pyrolyzed at 800°C.

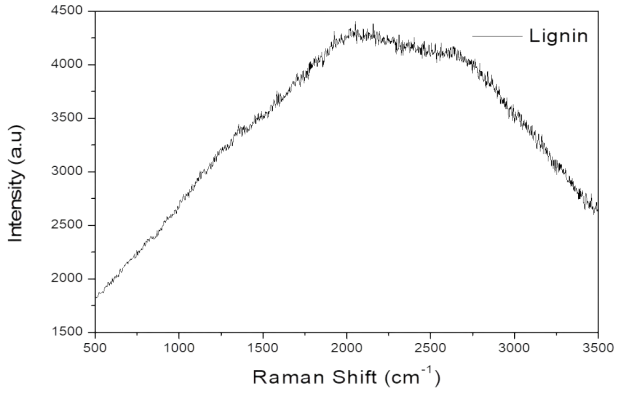

Figure 3: Raman spectra of commercial Lignin as received. Spectra were obtained using a Raman spectrometer with a 532nm laser excitation source.

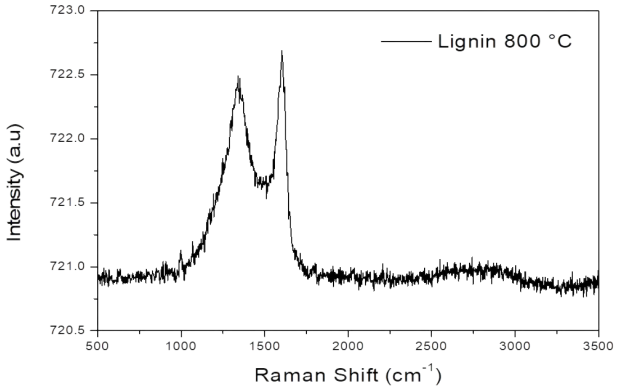

Figure 4: Raman spectra of pyrolysed at 800°C. Spectra were obtained using a Raman spectrometer with a 532nm laser excitation source.

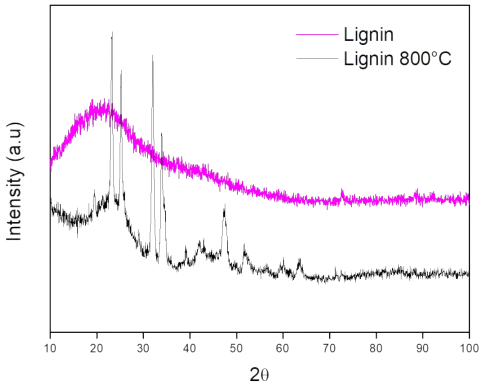

Figure 6: X-ray diffraction results of commercial Lignin and pyrolyzed at 800°C.

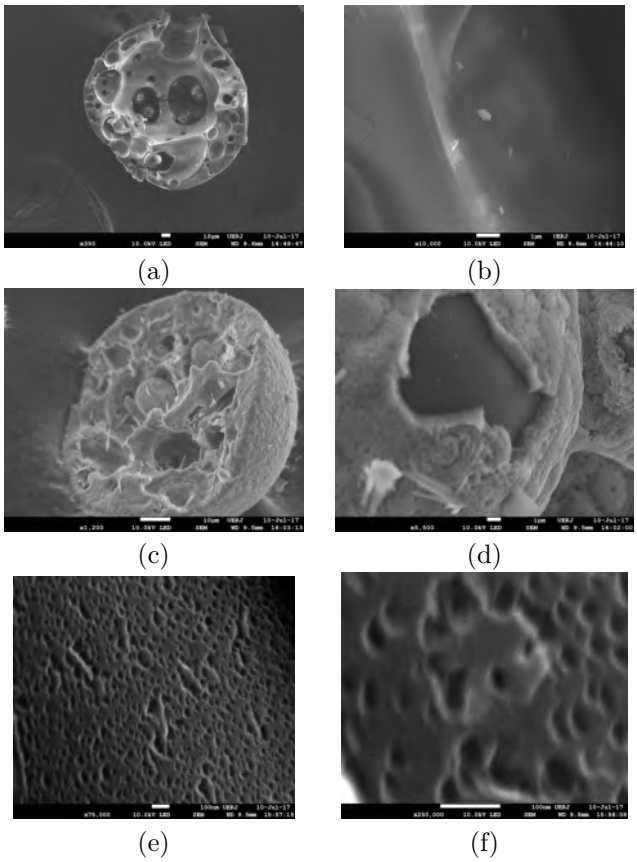

Figure 5: MEV - FEG images showing the differences between surfaces of Lignin as received (a),(b), and pyrolysed at 800°C (c), (d) and (e), (f) showing the appearance of pores at 800°C

4 Conclusions

Preliminary results after characterization of lignin as received and pyrolyzed at 800°C showed an increase crystallinity as shown in Raman spectroscopy Figs. 3 and 4 and X-ray diffraction Fig. 6. Increasing the surface area with the appearance of pores in the material (Fig. 5) this increase is very important for the physical adsorption that will be the majority mechanism in the lignin. The next step will be another characterization and adsorption tests on different types of lignin for a quantification of the amount of VOC's, like formaldehyde, can be adsorbed then after these characterization tests will be initiated studies for the formation of films by CVD (Chemical Vapour Deposition) process.

5 Acknowledgments

The authors would like to acknowledge financial support from FAPERJ and CAPES, and also to the SENAI group for the laboratory support.

References

[1] P. Gonugunta. Synthesis and characterization of biobased carbon nanoparticles from lignin. Master's thesis, University of Guelph, April 2012.

[2] P. Gonugunta, S. Vivekanandhan, A. K. Mohanty, and M. Misra. A study on synthesis and characterization of biobased carbon nanoparticles from lignin. *World Journal of Nano Science and Engineering*, 2: 148–153, 2012.

MAGNETIC CYCLES OF THE SUN AND ITS IMPACTS ON THE NATURAL PHENOMENA OF THE EARTH

Author: Lorena Albuquerque Santos[1]
Advisor(s): Prof. PhD Manoel Antônio da Fonseca Costa Filho[1]
Prof. PhD Antônio Guilherme Garcia Lima[1]
[1] State University of Rio de Janeiro

PPG-EM Seminars: season **2017**
www.ppg-em.uerj.br
November 22, 2017

Keywords: Sunspots, Solar cycles, Polar Aurora, Solar Protons

1 Introduction

The sun is a great mass of activity. With each period that lasts about 11 years, there is what is called the solar cycle. Within these cycles, there are two very important periods: the maximum and minimum solar. In the first period solar activities reach their highest point, ending the cycle. During the solar minimum, the sun does not become monotonous. Quite the opposite. During the minimum, it is possible to perceive some places where the magnetic field of the Sun opens, allowing the flow of particles, that affect Earth, causing geomagnetic storms. The remarks stemming from this article aims to find a possible correlation between the magnetic cycles of the Sun and some natural phenomena, such as intense and prolonged droughts, mainly those caused by phenomena such as El Niño and La Niña.

2 Methodology

The methodology to be used in this work is the bibliographical research, for future data analysis and construction of comparative and correlational tables.

3 Initial Analysis

The solar maximum of cycle 25 (current cycle) is expected to occur, according to NASA in 2022, and will be one of the weakest of all cycles. A weak solar cycle means you will not have to worry too much about solar flares or radiation storms. On the other hand, you will have to worry more about the cosmic rays. Cosmic rays are particles of high energy from space and able to traverse metals, plastic, human tissues and bones. For astronauts exposed to cosmic rays, the risk of developing cancer, cataracts and other diseases increases. Ironically, the solar explosions, which produce their own deadly radiation, displace the even more deadly cosmic rays. If the solar flares decrease, the cosmic rays intensify.

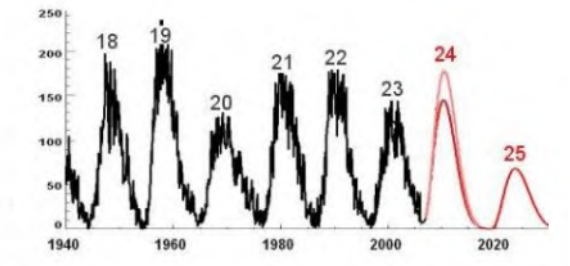

Figure 1: Number of Sunspots by year.

4 Events of Solar Protons

Solar proton levels reached dangerous levels during the intense storm named Halloween 2003. The following map shows the levels during the event on October 30, 2003. Proton levels reached 10 to 100 times the level of (orange) in much of North America and Europe at an altitude of 10,000 km (an average Earth orbit for satellites). These energy storms began, surprisingly, a total of two to three years after the solar maximum, when solar activity was declining. The map color coding shows proton levels 10 times or more below the warning level in blue, near the warning level in yellow, 10 times the warning level in green, and 10 to 1000 times the warning level in orange / red. The space operations division of the NOAA, Solar Proton Events (SEP) as dangerous ones with a proton flux greater than 10 MeV (million electron volts) or 10 pfu (particle flux units).

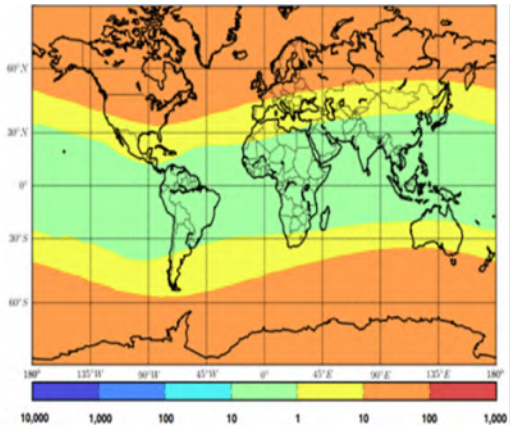

Figure 2: Blue: Safe, Green: Neutral, Red: Dangerous.

5 The Polar Aurora

The polar aurora is an optical phenomenon composed of a brightness observed in the night skies in the polar regions, due to the impact of particles of solar wind with the high atmosphere of the Earth, channeled by the terrestrial magnetic field. The energy source of the aurora is obtained by the solar winds flowing through the Earth. Both the magnetosphere and solar winds can conduct electricity. The solar wind and the magnetosphere are electrically conducting fluids with relative motion, and are capable of generating electric current, which gives rise to such a luminous effect.

Figure 3: This scary dawn was spotted near Nome in Alaska on October 14, 2003. Credits: John Russell.

6 Solar Storms

The release of energy is associated with sunspots, where events of great intensity occur. Solar storms release large amounts of particles that spread through the solar system, reaching even more distant planets.

7 Firsts Conclusions

Coronal mass ejections release large quantities of matter and electromagnetic radiation into space. Exhausted ionized gas may not move away from the solar corona (constituting a solar prominence) or go to the planetary orbits, being part of the solar wind. The expelled matter is a plasma consisting mainly of electrons and protons, but may contain small amounts of heavier elements, such as helium, oxygen and even iron. They are associated with major changes and disturbances of the coronal magnetic field. The solar wind is the continuous emission of charged particles from the solar corona. When explosions occur on the surface of the Sun, radiation emanation increases and the density of charged particles grows, which generates a magnetic storm that deforms the magnetosphere and produces phenomena such as the polar auroras. The exact mechanism of solar wind formation is not known to be composed of plasma of electrons, protons, sub-particles, and charged particles of heavier ionized atoms which are presumably accelerated by the thermonuclear reactions of the Sun in all directions and at high speeds. When solar flares are violent, they can result in geomagnetic storms on Earth; these directly influence the climate of the planet.

References

[1] U.S. NATIONAL AERONAUTICS and SPACE ADMINISTRATION. Solar minimum is coming. https://science.nasa.gov/science-news/news-articles/solar-minimum-is-coming, . Accessed: Nov 20, 2017.

[2] U.S. NATIONAL AERONAUTICS and SPACE ADMINISTRATION. The sun's magnetic field is about to flip. https://science.nasa.gov/science-news/science-at-nasa/2013/05aug_fieldflip, . Accessed: Nov 20, 2017.

[3] U.S. ATMOSPHERIC and ENVIRONMENTAL RESEARCH. Aer solar energetic proton nowcast: Examples and technical overview. http://www.aer.com/science-research/space/space-weather/solar-energetic-proton-nowcast/sep-nowcast-technical-overview. Accessed: Nov 20, 2017.

[4] U.S. WIKIPEDIA. Solar wind. https://en.wikipedia.org/wiki/Vento_solar, . Accessed: Nov 20, 2017.

[5] U.S. WIKIPEDIA. Aurora polar. https://pt.wikipedia.org/wiki/Aurora_polar, . Accessed: Nov 20, 2017.

STUDY OF EROSION BY IMPACT OF SOLID PARTICLES ON METALLIC COATING OBTAINED BY THERMAL ASPERSION

Author: Márcio Cossenza[1] marciocossenza@uol.com.br
Advisor: Marília Garcia Diniz[1]
[1]State University of Rio de Janeiro

November 29, 2017
PPG-EM Seminars: season **2017**
www.ppg-em.uerj.br

Keywords: Erosion, Metallic Coating, Thermal Spraying.

1 Introduction

In thermoelectrical plants, the generation of electric energy is based on the steam production from thermal energy. Some plants use mineral coal as fuel to keep the pressure that moves the generators.
In these kinds of plants, some problems are common in the boilers, due to the ashes of the coal. The erosion process takes place on the pipe walls, caused by the particles of ashes, composed basically by hard oxides.
The failures in acquatubular boilers happen on the pipe outer walls inside the combustion chambers of the boilers. The mechanism of degradation is a combination of corrosion and erosion, due to the impact of the ashes. The fan that feed the air into the combustion chamber is responsible for the velocity of the impact.
Some coatings have been developed along the decades to improve the resistance of the pipes against the degradation by the abrasive wear.
This paper has the objective to present the evaluation of a new metallic coating,in relation to abrasive wear. The metallic alloy is composed by Nb, B, Ni, Si, Mn, Al and Fe, with 13% of Chromium, obtained by arc spray method of thermal spraying process.
This method of application presents a porosity from 2% to 10% [1].
The erosion mechanism in laboratory conditions shall be as similar as possible to the real conditions, that occur in fact on the walls of pipes in acquatubular boilers.
This metallic coating was applied on the samples with the same composition, same application process and same parameters of the application that will be used on the pipes in the pressure vessels on the field.

2 Materials and Methods

The proposed process for evaluating the resistance of the coating uses alumina particles (Al2O3) as abrasive, flowing together with compressed air.
Inside the blasting chamber, a device was installed that allows the nozzle to be positioned with the correct distance of 10 milimeters to the sample, according to the standard ASTM G76.
This standard will be the direction of this test [2].
The support also can adjust the jet nozzle with different angles of attack (90°, 60°, 45°, 30°). These angles mean the ones between the axis of the nozzle and the surface of the plates used as samples, simulating the different directions of the ashes in real situation, between the region of the chamber from where the ashes come, with the tangent of the pipes.
A compact blasting chamber shown in the Figure 1 was coupled to the air compressor, similar to the common systems used in industrial processes of blasting [3].


Figure 1. Blasting chamber with the support inside

2.1 Target Material

The samples are presented as ASTM-A-178 steel plate with 8 mm thickness, and a 0.4 mm average thickness metallic alloy coating applied by thermal spraying process.
Few pieces of information are known about the mechanical strength of the coating material. Its microhardness was measured with the average value of 1042 HV.
Its density and level of porosity are unknown.

2.2 Shocking Particles

The alumina used is certified as 50 μm particles size.

2.3 Calibration of the Machine

The reference for the velocity used in the machine was made with the values established in ASTM G76 standard, defined as 0.0205 milligrams lost1020 carbon steel for each gram of abrasive alumina blasted, considering as 30 m/s the velocity of the particles. The machine was calibrated to achieve the same velocity of the particles as in the standard, for the 1020 steel samples, with the compressor output pressure equal 1.3 bar.

3 Results

After finishing the calibration of the machine, the blasting on the sampleswas started with the metallic coating.
On figure 2, it is possible to observe the impressions made by the alumina for the attack angles of 90, 60, 45, 30 degrees, on the samples covered by the alloy. Four samples were already blasted: the first on the top/left with three impressions with 90° attack angle; on the top/right with two 60° impressions; on the below/left with two 45° impressions; on the below/right with just one 30° impression.

Figure 2. Four samples already blasted

Figure 3 shows the comparison of the erosion rate with 90° angle of attack between the metal alloy and the A-178 steel substrate.

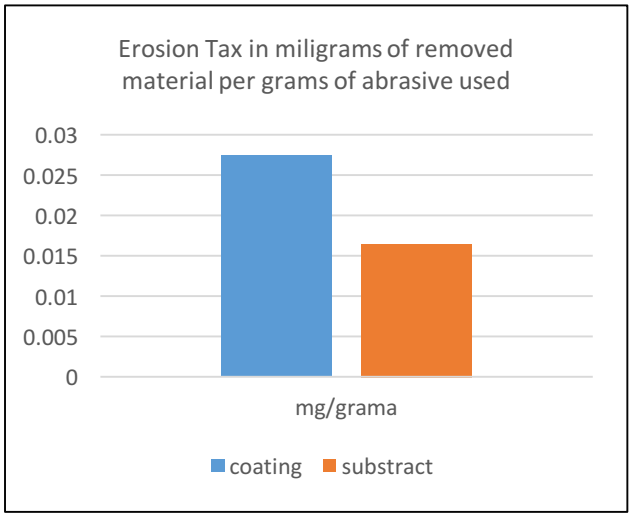

Figure 3: Erosion rate (mg/gram) of coating and substrate with 90 ° angle of attack.

Figure 4 shows the evolution of the erosion rate of the coating as function of the attack angle, from 30 to 90 degrees.

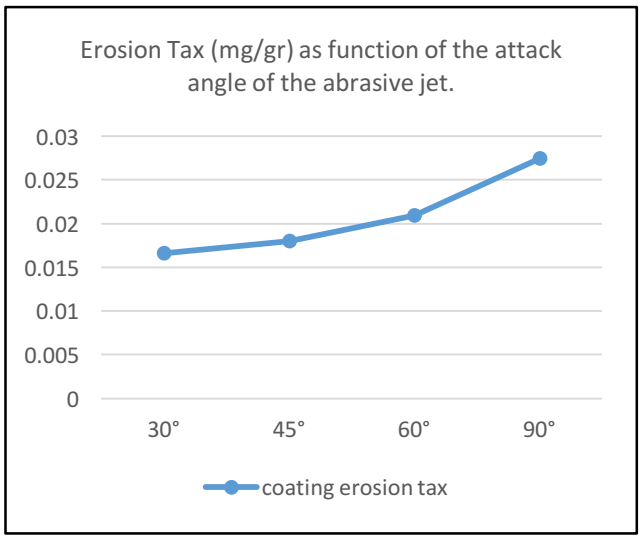

Figure 4. The difference of Erosive Tax when applied in different attack angles.

4 Conclusions

Based on the experiments carried on the samples, it was possible to observe, with the information presented on the figure 3, that the substract is more resistant than the coating, when both were blasted on laboratory conditions.
We must observe, on the thermal spraying process, that it leaves porosities in the coating material. It is possible that the lack of material could contribute for the erosion of final product.
The superficial roughness also is different from the ASTM-A178 plate received, laminated, and the coated surface, with a visible and considerable higher roughness.
Both the porosity and the roughness contributed for the less resistance of the coating, although the metallic alloy could present higher hardness than the ASTM-A178 carbon steel.
Also, it is possible to be observed, from the information of the figure 4, that the bigger angle, perpendicular to the surface, causes higher erosion rates than sharper angles.
Anyway, other tests shall be carried out, as corrosion test and thermal simulation, to evaluate if the coating configuration could be better in higher temperatures conditions.

References

[1] MORAIS, T.C. Estudo dos Processos de Aspersão Térmica em Materiais Metálicos de Forma a Auxiliar a Aplicação de Camadas para Diminuição de Desgastes e Corrosões na Superfície do Metal, Itajubá, 2016.

[2] ASTM G-76, Standard Test Method for Conducting Erosion Tests by Solid Particle Impingement Using Gas Jets, United States, 2005.

[3] ARAÚJO, A.C. Erosion by Impact of Solid Particles in Duplex Stainless Steel UNS S32205, Rio de Janeiro, 2015.

MANUFACTURE OF NANOPOSITIONERS FOR SCIENTIFIC AND INDUSTRIAL APPLICATIONS

Author: Rodrigo Sena Barbosa Leite[1] *rodrigoleite@mecanica.coppe.ufrj.br*
Advisor(s): Jose Brant de Campos[1]
[1] State University of Rio de Janeiro

PPG-EM Seminars: season **2017**
www.ppg-em.uerj.br
December 06, 2017

Keywords: nanopostioner, nanotecnology, microscope, piezoelectric

1 Introduction

Nanostructures in diverse material systems are the focus of research in various groups around the world, as not only new properties can be revealed, but also knowledge about processes already consolidated industrially can be revisited. Phenomena related to the dimensionality of matter are extremely relevant whether in industrial catalysts such as the physicochemical mechanisms of reaction of molecules on surfaces or in pigments used since the middle ages in which nano particles of copper, silver and gold are responsible for the observed colors [2]. Researches involving nano materials generally seek the correlation between functional macroscopic properties with their chemical, crystalline and morphological nature. For this reason, the development and innovation in nanotechnologies are dedicated to the combination of microscopy and spectroscopy with nanometric.

The project proposes the development and manufacture of a nano positioning device for instrumentation in microscopy and spectroscopy in low temperature and ultra high vacuum conditions. The innovative potential of the device will allow the development of a high value-added nanotechnology product in an industry still incipient in Brazil. This project seeks to integrate applied science in the development of a device with great future marketing potential and basic science creating conditions for scientific discovery in nano science, through the use of this device in probe and electronic microscopes. The main focus is on the experimental work, with the development of the nanopositioner designs, the mechanical fabrication and the performance of practical tests, as well as some characterizations of the generated device.

2 Methodology

Based on studies of existing nanopositioners and adapted to the size of piezoelectric ceramic, as well as to meet the size required for applications in microscopy, it was thought an unprecedented and functional design. The positioner was then designed using the solidworks software and then started machining in the CBPF machine manufactory.

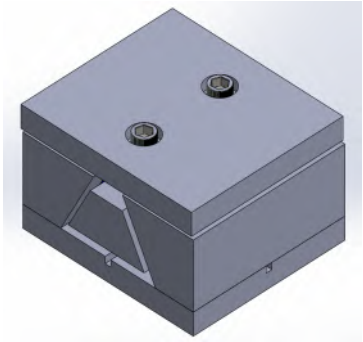

Figure 1: Isometric view of the nanopositionerr generated on solidworks.

In order to move the positioner it is necessary to use an electronic capable of generating voltage and couple the piezoelectric ceramics, which will receive the tension, contracting or expanding and thus generating the movement[3].

In addition, to couple the piezos, care must be taken with the temperature, since the glue needs to be heated but the piezos lose their properties if they are heated up to a certain temperature. Polishing will be carried out to improve the rough shape after machining and also facilitate the operation. A software of the electronic was installed, which allows controlling the movements of the positioner through a computer.

3 Results

The positioner has been successfully produced and is in the final stage of assembly, where the polishing was done to facilitate the movement. Afterwards, the piezos will be coupled with epoxy glue and connected in the electronics to move. A calibration will be done using an optical microscope.

The piezos need to be ”stacked” to perform the movement in the desired directions, for that an electrode is also used.

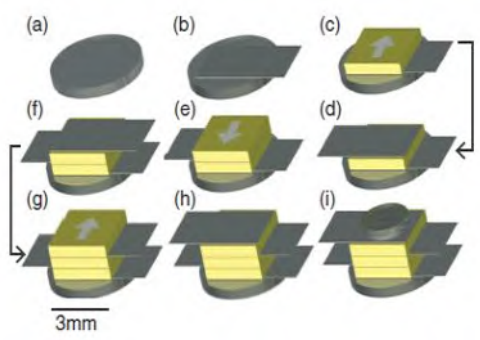

Figure 2: Example of building a piezoelectric stack. In (a) the base, in (b) an electrode is placed on the base with epoxy. In (c) the first piezo is inserted with the desired polarity. From (d) to (h) alternating electrodes and piezos are inserted. In (i) the last electrode enters and a sapphire plate is coupled [1]

After being completely complete, the positioner will be tested in STM (Scanning Tunneling Microscope) and its behavior will be evaluated in vacuum and at low temperatures.

4 Conclusions

In the first step, a design capable of moving samples in one dimension or up to 3 dimensions(when two or more positioners are coupled), was generated. In addition, more possibilities were opened:

- The main positioner is expected to be finalized in march 2018;
- Two prototype designs of other designs are ready and being evaluated;
- The goal would be to reduce the overall weight and measures of the device, when operated in more dimensions;
- Possibility of operating in all dimensions without the need of coupling;

5 Acknowledgments

The author thanks to the advisor Jose Brant de Campos and CBPF (Brazilian Center for Physical Research), including co-advisor Fernando Stavale, who provided the access and the partnership, as well as the CBPF team of researchers.

References

[1] K. R. Hairsine B. Drevniok, W. M. P. Paul and A. B. McLean. Methods and instrumentation for piezoelectric motors. Review of Scientific Instruments 83, 2012.

[2] V. Staemmler H-J. Freund, H. Kuhlenbecky. *Rep. Prog. Phys.*, 59:283, 1996.

[3] B. V. C Martins. *Desenho e construção de um UHV-STM.* Tese de doutorado, Unicamp, Sao Paulo, 2011.

CHARACTERIZATION AND PERFORMANCE ANALYSIS OF AISI1045 STEEL TOOL WITH TIN THINK FILM ON FSW WELDING PROCESS

Author: Paulo Rodrigues Oliveira[1] *rodrigues.oliveira@marinha.mil.br*
Advisor(s): Jose Bran de Campos[1]
[1] State University of Rio de Janeiro

PPG-EM Seminars: season **2017**
Dec 06, 2017 www.ppg-em.uerj.br

Keywords: FSW process, TiN think film, magnetron sputtering, plasma nitriding.

1 Introduction

The FSW (Friction Stir Welding process), consists in the realization of the union of materials, dissimilar or not, with the use of a rotating tool, responsible for the heating and mixing of the parts to be welded. Nowadays is been applied commercially in Al alloys but has been increasing your application in higher strength alloys, such as steel and Ti alloys. The absence of fusion ensures the weld joint elimination of defects common to conventional welding processes with melting puddles and cracks [3, 1]. The proposal of this work, developed by UERJ in conjunction with COPPE/UFRJ, PUC/RJ and CBPF/LABNANO, is the production of a tool dedicated to the FSW welding process applied to union of the Al alloy, series 5XXX.X with low cost and good period of life. AISI1045 steel coated with TiN was used as tool material for the tooling through the Magnetron Sputtering process.

2 Experimental Procedures

To obtain light and strength structures new process and materials there will be develop in engineering field, Fig. 1 shows the schematic diagram for FSW process.

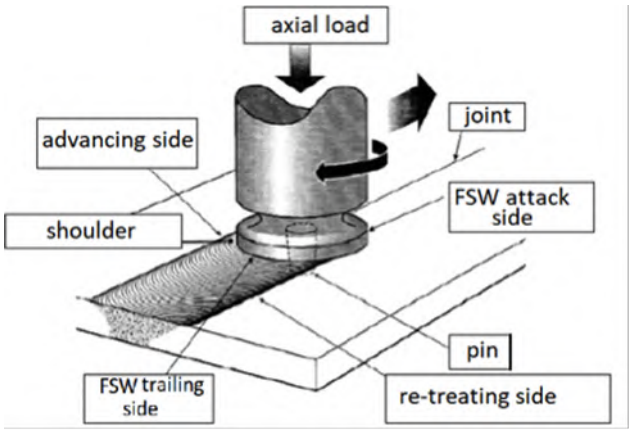

Figure 1: Schematic diagram for typical FSW process [3].

The FSW process highlights with a convenient tool for the metalworking industry, reach high production rates with low defects. For its execution are necessary:

1. Machine tool (milling machine);
2. Dedicated tool; and
3. The development of the tool and the criterions process to selection of its material is fundamental to the execution of the weld with perfection and obtaining a competitive product to the market.

AISI 1045 blasted steel samples, grade A/SA 3, received the ionic nitriding process and deposition of TiN film in a non-reactive atmosphere. For the execution of both processes a Magnetron Sputtering reactor developed and built in CBPF/LABNANO was used. The use of the same reactor to perform both activities reduces operational costs and eliminates possible contamination between processes. The need for ionic nitriding prior to deposition of the TiN film is a function of the difference between the H/E ratio of the materials, film and substrate. For AISI 1045 steel the H/E ratio is 0.009 and for TiN is 0.04. This difference is responsible for failure between the film/substrate adhesion. Tables 1 and 2 present the values of the parameters used for the plasma nitriding and TiN deposition processes. The values were obtained to avoid the formation of the white layer, nitriding, and homogeneity of the TiN film. The electrical source used in all cases was RF.

Mat.	Tar.	Pow.	Pr.	Gas	Tem.	Rate
Si	TiN	50	5	Ar	amb.	0
Steel/Si	TiN	100	5	Ar	amb.	1.01
Steel/Si	TiN	100	5	Ar	550	1.101
Si	TiN	175	5	Ar	550	1.152

Table 1: Plasma nitriding parameters.

The abbreviated labels of Table 1 columns abbreviated refer successively to: material, target, power[W], press[mTorr], gas, temperature of the substance[^{o}C] and rate[nm/min].

Stage.	Gas	Tem.	t.	Pr.	Po.
Etching	100%Ar	350	15	100	30
Nitride	20%N_2-80%Ar	350	60	$\frac{160N_2}{590Ar}$	1.01

Table 2: TiN Deposition rates.

The abbreviated labels of Table 2 columns refer successively to: stage, gas concentration, temperature of the substance[^{o}C], time[min] and power[W].

3 Results and Discussion

The values obtained by the characterization processes performed agree with the bibliographic references [2]. The HV hardness values indicate that nitriding was performed without the formation of typical white layer compounds, brittle high hardness nitrides. Fig. 2 shows the results obtained for the hardness test.

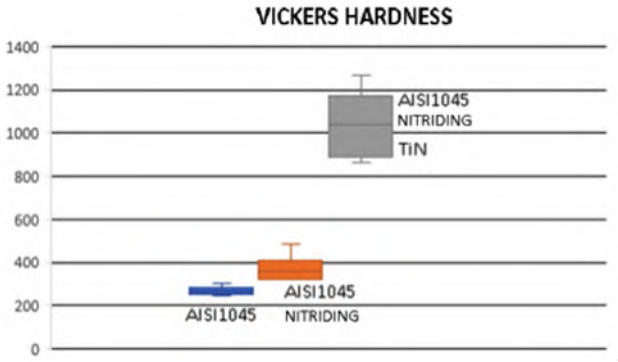

Figure 2: Values for Vickers Hardness test.

Fig. 3 shows the diffractogram for the TiN coated sample.

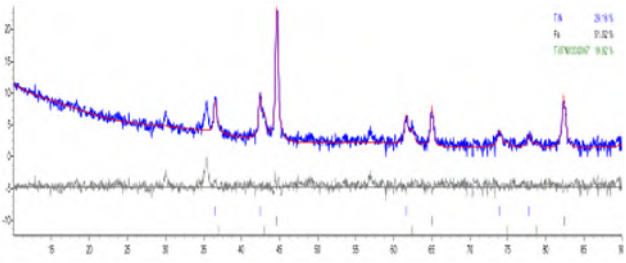

Figure 3: Diffractogram shows the compounds after TiN deposition TiN(29,16%), Fe(51,02%) and $Ti_{0,7}N_{0,33}O_{0,64}$(19,82%).

4 Conclusions

The processes of nitriding and deposition of TiN in the same equipment were viable. Performance tests with the tool were performed and the preliminary analysis showed an effective use of TiN. The formation of TiNO indicates contamination of the film with O_2. Impurities in the chamber or contamination of the atmosphere are among the hypotheses for contamination. Methods to avoid this contamination should be applied.

5 Acknowledgments

The authors thank to

- UERJ/NANOFAB for the technical support;
- CBPF/LABNANO, UFRJ/COPPE and PUC/RIO for their support and partnership.

References

[1] Karen Johanna Quintana Cuellar, Harry Mitrogiannopoulos, Daniel Hiller, Daniel Trimble, Rocco Lupoi, Garret O'Donnell, Jose Luis Silveira, and Shaun McFadden. A study on internal defects in friction stir welding of aluminium alloys. In *Proceedings of 31st International Manufacturing Conference (IMC31)*. Cork Institute of Technology, September 2014.

[2] Adonias Ribeiro Franco Júnior. *Obtenção de Revestimento Dúplex por Nitretação a Plasma e PVD TiN em Aços Ferramenta AISI D2 e AISI H13*. PhD thesis, Escola Politécnica da Universidade de São Paulo, 2003.

[3] R S Mishra and Z Y Ma. Friction stir welding and processing. *Material Science and Engineering*, R50: 1–78, 2005.